Electronic Supplementary Material (ESI) for Chemical Science.
This journal is © The Royal Society of Chemistry 2024

Electronic Supplementary Information (ESI)

Controllable π-π Coupling of Intramolecular Dimer Models at Aggregated State

Qiuyan Liao[a], Aisen Li[b], Arui Huang[a], Jiaqiang Wang[c], Kai Chang[a], Hehua Li[a], Pengfei Yao[a], Cheng Zhong[a], Peidong Xie[a], Jinfeng Wang[c], Zhen Li*[a, b, c], Qianqian Li*[a]

[a] Hubei Key Lab on Organic and Polymeric Opto-Electronic Materials, TaiKang Center for Life and Medical Sciences, Department of Chemistry, Wuhan University, Wuhan 430072, China.
[b] Joint School of National University of Singapore and Tianjin University, International Campus of Tianjin University, Fuzhou, 350207, China;
[c] Institute of Molecular Aggregation Science, Tianjin University, Tianjin 300072, China.

Contents

1. Experiment section 4

Scheme S1. Molecular structures and edge-to-face T-shaped packing modes 4

1.1. Materials 4

1.2. Instruments 4

1.3. Theoretical Calculation 5

1.4. Synthetic procedures 5

Scheme S2. Synthetic routes 5

2. Additional data and spectra 8

Fig. S1-12 ^{1}H NMR and ^{13}C NMR spectra of X1R and X2R derivatives 8

Fig. S13 Absorption spectra of X1R and X2R derivatives in THF solution at room temperature 14

Fig. S14 Molecular geometry in X2B, X2N and X2A crystal 14

Fig. S15 Fluorescence decay of X2A in different solution at room temperature 14

Fig. S16 PL spectra of X1R and X2R derivatives in solution with different polarity 15

Fig. S17 PL spectra of X1A in THF solution with different concentration 15

Fig. S18 PL spectra of X2A in THF solution with different concentration 15

Fig. S19 PL spectra of X1R abd X2R crystals at room temperature 16

Table S1 Photophysical properties of X1R and X2R derivatives at room temperature. 16

Fig. S20-25 Intermolecular interactions in X1R and X2R crystals 17

Table S2 Structural data of single crystals based on X1R and X2R derivatives 20

Table S3 Intermolecular interactions of X1R and X2R crystals at room temperature. 21

Fig. S26 Absorption spectra of X2A crystals 21

Fig. S27 Fluorescence decay of X2A crystals at room temperature. 22

Fig. S28 Absorption spectra of X2A compound in different solution 22

Table S4 Photophysical properties of X2A crystals at room temperature. 22

Fig. S29 Molecular packing modes of polymorphs of X2A crystals 23

Fig. S30 Intermolecular interactions between X2A molecule and solvent molecules 23

Fig. S31 Raman spectra of X2A-B-$ClCH_2CH_2Cl$ and X2A-G crystal 24

Fig. S32 Micro-infrared spectra of X2A-B-$ClCH_2CH_2Cl$ and X2A-G crystal 24

Fig. S33 Emission images of X2A crystals cultivated from different solvents 25

Fig. S34 PL spectra of X2A crystals cultivated from different solvents 25

Fig. S35 Crystal structures of X2A crystals cultivated from different solvents 26

Table S5 CCDC numbers of X2A crystals 26

Fig. S36 PL spectra of X2A-B-$ClCH_2CH_2Cl$ crystal at different temperature 27

Table S6 Photoluminescence properties of X2A crystals at different temperature 27

Fig. S37 Fluorescence decay of X2A-B-$ClCH_2CH_2Cl$ crystal at different temperature 27

Table S7 Photoluminescence lifetimes of X2A crystals at different temperature 28
Fig. S38 PXRD patterns of X2A-B-$ClCH_2CH_2Cl$ crystals and X2A-G crystal....28
Fig. S39 PL spectra and fluorescence images of X2A-B-CH_2Cl_2 crystal at different temperature. 29
Fig. S40 ^1H NMR spectra of X2A-B-CH_2Cl_2 crystal at different states 29
Fig. S41 PL spectra of X2A-G crystal at different temperature 30
Fig. S42 TGA analysis of X2A powder. 30
Fig. S43 DSC curves of X2A-B-$ClCH_2CH_2Cl$, X2A-B-CH_2Cl_2 and X2A-G crystal 30
Table S8 Intermolecular interactions and calculated interaction energy between solvent and anthracene moiety....31
Fig. S44 Distances of intermolecular interactions between solvent and anthracene moiety 31
Fig. S45 ^1H NMR spectra of X2A-B-$ClCH_2CH_2Cl$ crystal before and after grinding....31
Fig. S46 PL spectra of X2A-B-$ClCH_2CH_2Cl$ crystal upon mechanical force....32
Fig. S47 Patterns constructed by X2A-B microcrystal 32
Fig. S48 PL spectra of X2A-B-$ClCH_2CH_2Cl$ crystal with isotropic compression....33
Fig. S49 The fluorescence property of X2A-B-$ClCH_2CH_2Cl$ crystal with the release of pressure 33
Fig. S50 The fluorescence property of X2A-G crystal with isotropic compression....34
Fig. S51 The fluorescence property of X2A-G crystal with the release of pressure 34
Fig. S52 Raman spectra of X2A-B-$ClCH_2CH_2Cl$ crystal under different pressure 35
Fig. S53 Raman spectra of X2A-G crystal under different pressure 35
Fig. S54 The fluorescence property of X2A-B-CH_2Cl_2 crystal under different pressure 36
Fig. S55 Raman spectra of X2A-B-CH_2Cl_2 crystal under different pressure 36
Fig. S56 Molecular packing modes of X2A-B-$ClCH_2CH_2Cl$ and X2A-G crystal 37
Table S9 Molecular configuration of X2A-B-$ClCH_2CH_2Cl$ and X2A-G crystal....37
Fig. S57 Interaction energy of X2A-B-$ClCH_2CH_2Cl$ crystals at different temperature....38
Table S10 Interaction energy of X2A-B-$ClCH_2CH_2Cl$ crystals at different temperature....38
Fig. S58 The scatter diagram for RDG of X2A-B-$ClCH_2CH_2Cl$ and X2A-G crystal 39
Fig. S59 Electrostatic potential analysis of X2A-B-$ClCH_2CH_2Cl$ and X2A-G crystal....39
Fig. S60 Gradient isosurfaces for X2A-B-$ClCH_2CH_2Cl$ crystals and X2A-G crystal 40
Table S11 Transfer integrals of X2A-B-$ClCH_2CH_2Cl$ and X2A-G crystal 40
Fig. S61 HOMO, LUMO orbits of X2A-B-$ClCH_2CH_2Cl$ and X2A-G crystal 41
Fig. S62 The geometries of I-VI 41
Reference....41

1 Experiment section

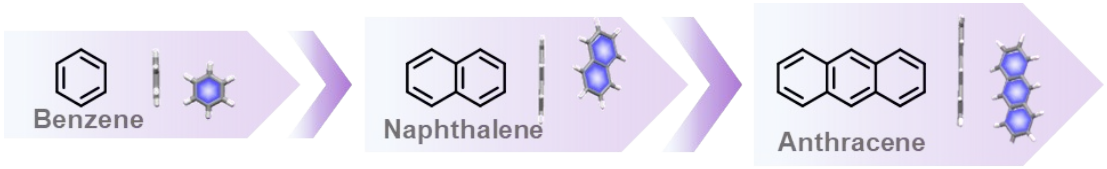

Scheme S1. Molecular structures and edge-to-face T-shaped packing modes of benzene, naphthalene, and anthracene.

1.1 Materials.

1,4-Dioxane, tetrahydrofuran, deionized water were purged with nitrogen before use. All other solvents, 9,9-dimethylxanthene, 2-chloro-2-methylpropane, bromine, phenylboronic acid, 1-naphthaleneboronic acid and 9-bromoanthracene were purchased and used directly as received. 9,9-dimethylxanthene and 2-chloro-2-methypropane were purchased from Aladdin. Bromine was purchased from Shanghai Lingfeng Chemical Reagent Co., Ltd. Phenylboronic acid was purchased from Soochiral Chemical Science & Technology Co., Ltd. 1-naphthaleneboronic acid and 9-bromoanthracene were purchased from Energy Chemical.

1.2 Instruments

^{1}H and ^{13}C NMR spectra were recorded on a Bruker Avance III HD 400 MHz or Avance NEO 400 MHz digital NMR spectrometer using tetramethylsilane (TMS; δ = 0 ppm) as internal standard. Mass spectra were measured on a ZAB 3F-HF mass spectrophotometer and LCQ advantage electrospray mass spectrometer. Elemental analyses were performed by a VARIO EL III element analyzer. UV-vis spectra were conducted on a Shimadzu UV-2550 spectrometer. PL spectra were performed on a Hitachi F-4600 fluorescence spectrophotometer and an Ocean Optics QE65 Pro spectrometer (Ocean Optics, Inc., Dunedin, FL, United States). Quantum yields and lifetimes at room temperature were determined with FLS 980 spectrometer. The powder X-ray diffraction patterns were recorded by D8 Advanced (Bruker) using Cu-Kα radiation from 5 ° to 60 °. The single-crystal X-ray diffraction data of X1B, X2B, X1N, X2N, X1A, X2A-B-$ClCH_2CH_2Cl$, X2A-B-CH_2Cl_2, X2A-B-CH_2Br_2, X2A-B-CH_3I and X2A-G crystals at room temperature were collected in a Bruker Smart Apex CCD diffractometer and Bruker D8 VENTURE. Micro photoluminescence spectra were measured by analyzing system (HORIBA iHR 320 detector was coupled to the Olympus IX71/IX5 microscope, 360 nm UV laser Changchun New Industries). Micro-infrared spectra were performed on Nicolet IN10 Thermo Fisher Scientific Infrared Microscope. PL spectra and lifetimes of X2A-B-$ClCH_2CH_2Cl$ crystal at different temperature were performed with FLS 980 spectrometer. The single-crystal X-ray diffraction data of X2B at different temperature were collected in Rigaku XtaLAB Synergy Custom. The high-pressure fluorescence spectra at room temperature were performed on a fluorescence microscope (IX71, Olympus 20×, numerical aperture=0.4) equipped with a spectrometer (Horiba Jobin Yvon iHR320), with a light source of mercury lamp (with 365 nm excitation wavelength). The measurement of the ruby chip was conducted at a Horiba Jobin Yvon T64000 Raman spectrometer with a 1800 gr/mm holographic grating and the excitation wavelength from laser is 532 nm line. High-pressure Raman spectra were acquired at a confocal Raman system, which is based on an optical microscope (LabRAM Aramis, Horiba JobinYvon) constructed with the excitation laser of 633 nm and 785 nm (the power of 20 mW), a 50×/0.75 NA microscope objective, and a standard CCD array detector.

1.3 Theoretical Calculation

TD-DFT calculations were performed on Gaussian 16 program (Revision A.03)[1] and Gaussian 16 (Revision C.01). The geometries were extracted from single crystal. The HOMO, LUMO orbits and energy gaps for the isolated molecules were performed with the Becke's three-parameter exchange functional along with the Lee Yang Parr's correlation functional (B3LYP) using 6-31G (d) basis sets. The electrostatic potential (ESP) images were obtained from Gaussian

View 6 with electron density isosurface value of 0.001. The interaction energies were calculated based on B3LYP/6-31G(d) basis sets, and the NCI analysis was conducted through Multiwfn 3.8[2], VMD and gnuplot programs (isosurface value of 0.8). The transfer integral was investigated based on anaconda2 package with the same method. The potential energy surface (PES) was scanned based on B3LYP/6-31G(d) basis sets.

1.4 Synthetic procedures

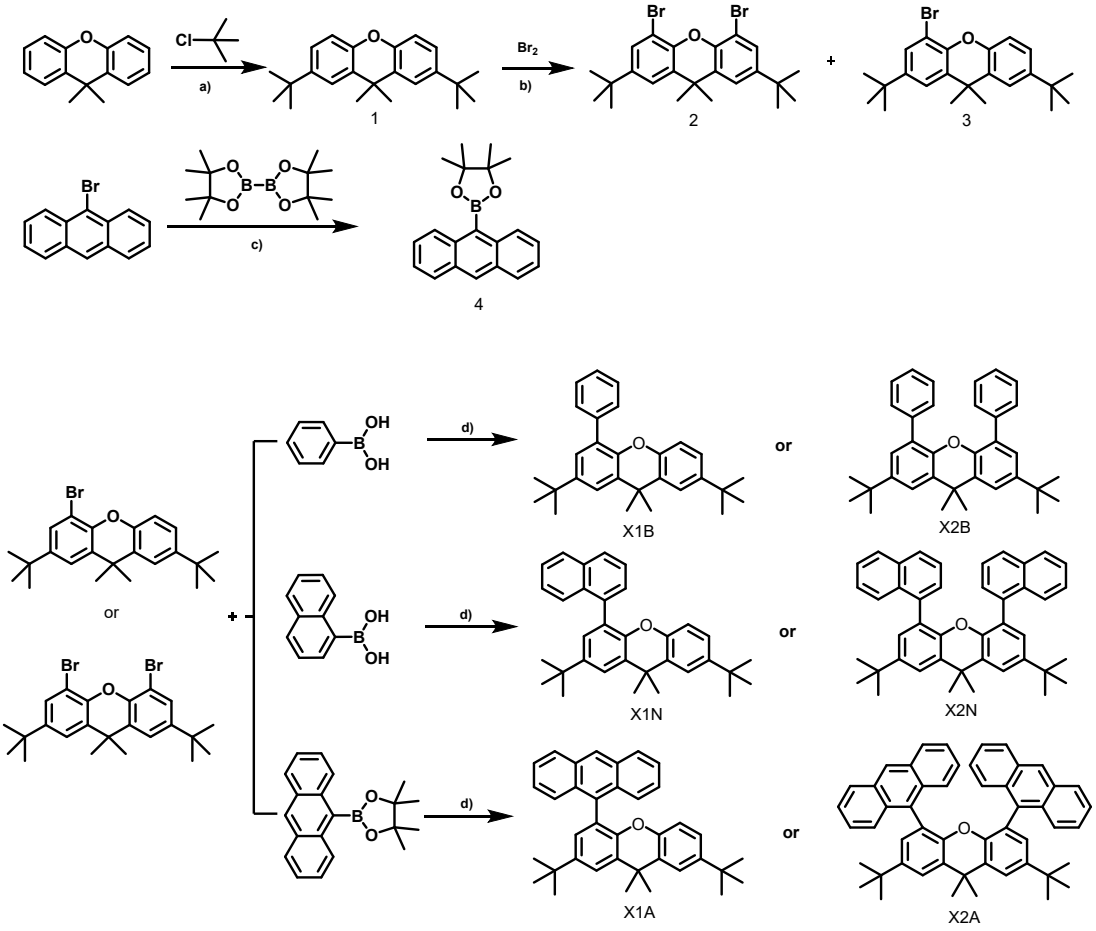

Scheme S2. Synthetic routes of compound X1R and X2R. Synthetic routes of compound X1B, X2B, X1N, X2N, X1A and X2A. Conditions: a): $FeCl_3$, CH_2Cl_2, 15 h; b): $CHCl_3$, 12h; c) KOAc, 1, 4-dioxane, $Pd(dppf)Cl_2$, reflux, 24 h; d): K_2CO_3, Bis (di-tert-butyl(4-dimethylaminophenyl) phosphine) dichloropalladium (II) (887919-35-9), tetrahydrofuran, deionized water, reflux, 12 h.

Intermediate compound 1. 9,9-Dimethylxanthene (3.00 g, 14.30 mmol) and $FeCl_3$ (0.116 g, 0.72 mmol) were dissolved in dichloromethane (15 mL) and then stirred at 0 °C. Then 1.8 mL 2-chloro-2-methylpropane was dissolved in dichloromethane (15 mL) and added dropwise to 9,9-dimethylcanthene solution with a constant pressure drop funnel, which was allowed to warm up to room temperature over 3 h, and stirred for another 15 h. The reaction mixture was quencwithd by water, then extracted with CH_2Cl_2. The combined organic layer was dried over anhydrous Na_2SO_4 and concentrated by rotary evaporation. The crude product was purified by silica gel column chromatography using petroleum ether as eluent, and obtained as a white solid (3.23 g, 70%). ^{1}H NMR (400 MHz, $CDCl_3$) δ (ppm): 7.40 (d, *J* = 2.2 Hz, 2H, ArH), 7.21 (d, *J* = 2.2 Hz, 1H, ArH), 7.19 (d, *J* = 2.2 Hz, 1H, ArH), 6.97-6.94 (m, 2H, ArH), 1.65 (s, 6H, -CH_3), 1.33 (s, 18H, -CH_3). ^{13}C NMR (100 MHz, $CDCl_3$) δ (ppm): 148.34, 145.41, 129.23, 124.34, 122.69, 115.66, 34.48, 34.39, 32.57, 31.62.

Intermediate compound 2. Compound 1 (2.00 g, 6.20 mmol) was dissolved in chloroform (25 mL) and then stirred at 0 °C. Bromine (1.36 mL, 24.80 mmol) was diluted by chloroform (12 mL) and then added dropwise to above mentioned

solution with a constant pressure drop funnel and then the reaction mixture was slowly warmed to room temperature and stirred for another 12 h. The reaction mixture was quenched by saturated Na_2SO_3 solution, then extracted with CH_2Cl_2. The combined organic layer was dried over anhydrous Na_2SO_4 and concentrated by rotary evaporation. The crude product was purified by silica gel column chromatography using petroleum ether as eluent, and obtained as a white solid (2.83 g, 95%). ^{1}H NMR (400 MHz, $CDCl_3$) δ (ppm): 7.47 (d, *J* = 2.2 Hz, 2H, ArH), 7.33 (d, *J* = 2.3 Hz, 2H, ArH), 1.62 (s, 6H, -CH_3), 1.32 (s, 18H, -CH_3). ^{13}C NMR (100 MHz, $CDCl_3$) δ (ppm): 147.26, 145.29, 131.15, 128.48, 121.56, 110.42, 35.78, 34.64, 31.88, 31.43.

Intermediate compound 3. Compound 1 (1.00 g, 3.10 mmol) was dissolved in chloroform (25 mL) and then stirred at 0 °C. Bromine (0.16 mL, 3.10 mmol) was diluted by chloroform (6 mL) and then added dropwise to above mentioned solution with a constant pressure drop funnel. After the addition of bromine, the reaction mixture was slowly warmed up to room temperature and stirred for another 12 h. The reaction mixture was quenched by saturated Na_2SO_3 solution, then extracted with CH_2Cl_2. The combined organic layer was dried over anhydrous Na_2SO_4 and concentrated by rotary evaporation. The crude product was purified by silica gel column chromatography using petroleum ether as eluent, and obtained as a white solid (0.93 g, 75%). ^{1}H NMR (400 MHz, $CDCl_3$) δ (ppm): 7.44 (d, *J* = 2.3 Hz, 1H, ArH), 7.38 (d, *J* = 2.3 Hz, 1H, ArH), 7.34 (d, *J* = 2.2 Hz, 1H, ArH), 7.23 (dd, *J* = 8.5, 2.3 Hz, 1H, ArH), 7.09-7.07 (m, 1H, ArH), 1.63 (s, 6H, -CH_3), 1.33 (s, 9H, -CH_3), 1.32 (s, 9H, -CH_3). ^{13}C NMR (100 MHz, $CDCl_3$) δ (ppm): 148.14, 146.47, 146.15, 145.29, 131.35, 129.01, 128.23, 124.49, 122.30, 121.94, 116.07, 109.97, 35.09, 34.55, 34.52, 32.19, 31.57, 31.43.

Intermediate compound 4. 9-Bromoanthracene (1.00 g, 3.89 mmol), Pd(dppf)Cl_2 (0.20 g, 0.27 mmol), 4,4,4',4',5,5,5',5'-octamethyl-2,2'-bi(1,3,2-dioxaborolane) (1.48 g, 5.84 mmol) and KOAc (0.76 g, 7.78 mmol) were added in a nitrogen flushed schlenk tube, deoxygenated 1,4-dioxane was added and the mixture was stirred for 15 h under nitrogen atmosphere. The reaction mixture was filtered, the filtrate was washed with CH_2Cl_2, and the combined organic layer was dried over anhydrous Na_2SO_4 and concentrated by rotary evaporation. The crude product was purified by silica gel column chromatography using petroleum ether/dichloromethane (10/1) as eluent, and obtained as a yellow solid (0.83 g, 70%). ^{1}H NMR (400 MHz, $CDCl_3$) δ (ppm): 8.48-8.43 (m, 3H, ArH), 7.99 (d, *J* = 8.2 Hz, 2H, ArH), 7.50-7.42 (m, 4H, ArH), 1.58 (s, 12H, -CH_3). ^{13}C NMR (100 MHz, $CDCl_3$) δ (ppm): 135.93, 131.16, 129.52, 128.82, 128.34, 125.81, 124.90, 84.42, 25.21.

The general synthetic route of X1B, X1N and X1A. Compound 3 (1.0 equiv.), one of compounds 3-5 (2.0 equiv.), K_2CO_3 (2.0 equiv.), Bis(di-tert-butyl (4-dimethylaminophenyl) phosphine) dichloropalladium (II) (887919-35-9) (0.05 equiv.) were added in a nitrogen flushed schlenk tube, tetrahydrofuran (20 mL) was added and the mixture was bubbled with nitrogen for 30 min. Then the reaction was refluxed for 12 h before quenching by water. The resultant mixture was extracted with CH_2Cl_2, the combined organic layer was dried over anhydrous Na_2SO_4 and concentrated by rotary evaporation. The crude product was purified by silica gel column chromatography using petroleum ether or petroleum ether/dichloromethane (5/1) as eluent.

X1B. A white solid (0.38 g, 85%). ^{1}H NMR (400 MHz, $CDCl_3$) δ (ppm): 7.63-7.60 (m, 2H, ArH), 7.48-7.41 (m, 4H, ArH), 7.39-7.35 (m, 1H, ArH), 7.27-7.25 (m, 1H, ArH), 7.17 (dd, *J* = 8.5, 2.4 Hz, 1H, ArH), 6.89 (d, *J* = 8.5 Hz, 1H, ArH), 1.68 (s, 6H, -CH_3), 1.36 (s, 9H, -CH_3), 1.33 (s, 9H, -CH_3). ^{13}C NMR (100 MHz, $CDCl_3$) δ (ppm): 148.68, 145.65, 145.61, 145.17, 138.72, 130.39, 129.82, 129.63, 128.78, 127.98, 126.87, 126.03, 124.15, 122.16, 121.82, 115.74, 34.91, 34.55, 34.49, 31.87, 31.59. MS (EI, m/z): $[M]^+$ calcd for $C_{29}H_{34}O$, 398.26; Found, 398.15. Anal. Cacld for $C_{29}H_{34}O$: C, 87.39; H, 8.60; Found: C, 87.66; H, 8.41.

X1N. A white solid (0.13 g, 80%). ^{1}H NMR (400 MHz, $CDCl_3$) δ (ppm): 7.92-7.89 (m, 2H, ArH), 7.64 (dd, *J* = 8.4, 1.5 Hz, 2H, ArH), 7.59-7.55 (m, 1H, ArH), 7.52-7.45 (m, 3H, ArH), 7.41 (m, 1H, ArH), 7.36-7.32 (m, 1H, ArH), 7.25-7.22 (m, 1H, ArH), 7.05-7.03 (m, 1H, ArH), 6.44 (d, *J* = 8.5 Hz, 1H, ArH), 1.79 (s, 3H, -CH_3), 1.65 (s, 3H, -CH_3), 1.36 (s, 9H, -CH_3), 1.30 (s, 9H, -CH_3). ^{13}C NMR (100 MHz, $CDCl_3$) δ (ppm): 148.73, 146.45, 145.46, 145.09, 137.14, 133.50, 132.26, 130.21, 129.79, 128.03, 127.73, 127.64, 127.55, 127.12, 126.96, 125.67, 125.54, 125.39, 124.01, 121.91, 121.89, 116.08, 35.00, 34.58, 34.46, 32.70, 31.58, 30.80. MS (EI, m/z): $[M]^+$ calcd for: $C_{33}H_{36}O$, 448.65; Found, 448.20. Anal. Cacld for $C_{33}H_{36}O$: C, 88.35; H, 8.09; Found: C, 88.44; H, 8.05.

X1A. A white solid (0.37 g, 60%). ^{1}H NMR (400 MHz, $CDCl_3$) δ (ppm): 8.53 (s, 1H, ArH), 8.07 (d, *J* = 8.5 Hz, 2H, ArH), 7.67-7.60 (m, 3H, ArH), 7.47-7.40 (m, 3H, ArH), 7.32-7.28 (m, 2H, ArH), 7.21 (d, *J* = 2.3 Hz, 1H, ArH), 6.95 (dd, *J* = 8.5, 2.4 Hz,

1H, ArH), 6.22 (d, *J* = 8.5 Hz, 1H, ArH), 1.76 (s, 6H, -CH_3), 1.36 (s, 9H, -CH_3), 1.28 (s, 9H, -CH_3). ^{13}C NMR (100 MHz, $CDCl_3$) δ (ppm): 148.73, 147.14, 145.35, 145.09, 133.94, 131.50, 130.57, 130.26, 129.64, 128.31, 128.09, 127.16, 126.48, 125.17, 124.98, 123.96, 122.02, 121.88, 116.10, 35.01, 34.63, 34.42, 31.92, 31.66, 31.62, 31.55. MS (ESI, m/z): $[M+H]^+$ calcd for: $C_{37}H_{38}O$, 498.3; Found, 499.3. Anal. Cacld for $C_{37}H_{38}O$: C, 89.11; H, 7.68; Found: C, 88.97; H, 7.72.

The general synthetic route of X2B, X2N and X2A. Compound 2 (1.0 equiv.), one of Compound 3-5 (3.0 equiv.), K_2CO_3 (4.0 equiv.), Bis(di-tert-butyl (4-dimethylaminophenyl) phosphine) dichloropalladium (II) (887919-35-9) (0.05 equiv.) were added in nitrogen flushed round bottom flask, tetrahydrofuran (20-40 mL) was added and the mixture was bubbled with nitrogen for 30 min. Then the reaction was refluxed for 12 h before quenching by water. The resultant mixture was extracted with CH_2Cl_2, the combined organic layer was dried over anhydrous Na_2SO_4 and concentrated by rotary evaporation. The crude product was purified by silica gel column chromatography using petroleum ether and dichloromethane (10/1) as eluent.

X2B. A white solid (0.79 g, 80%). ^{1}H NMR (400 MHz, $CDCl_3$) δ (ppm): 7.43 (d, *J* = 2.4 Hz, 2H, ArH), 7.26-7.25 (m, 4H, ArH), 7.21-7.18 (m, 4H, ArH), 7.12-7.08 (m, 4H, ArH), 1.73 (s, 6H, -CH_3), 1.35 (s, 18H, -CH_3). ^{13}C NMR (100 MHz, $CDCl_3$) δ (ppm): 146.21, 145.35, 138.26, 130.67, 129.61, 129.35, 127.80, 126.40, 126.05, 121.24, 35.27, 34.56, 31.59, 31.34. MS (EI, m/z): $[M]^+$calcd for: $C_{35}H_{38}O$, 474.29; Found, 474.86. Anal. Cacld for $C_{35}H_{38}O$: C, 88.56; H, 8.07; Found: C, 88.12; H, 8.29.

X2N. A white solid (0.90 g, 75%). ^{1}H NMR (400 MHz, $CDCl_3$) δ (ppm): 7.73 (s, 2H, ArH), 7.48-7.43 (m, 6H, ArH), 7.36 (t, *J* = 7.4 Hz, 2H, ArH), 7.30-7.29 (m, 2H, ArH), 7.25-7.19 (m, 2H, ArH), 6.88 (d, *J* = 8.4 Hz, 2H, ArH), 1.78 (s, 6H, -CH_3), 1.38 (s, 18H, -CH_3). ^{13}C NMR (100 MHz, $CDCl_3$) δ (ppm): 144.72, 135.57, 132.97, 131.74, 127.97, 127.65, 126.99, 126.88, 126.77, 126.07, 125.11, 124.87, 124.67, 124.56, 124.15, 121.66, 35.15, 34.54, 32.43, 31.57. MS (EI, m/z): $[M]^+$calcd for: $C_{43}H_{42}O$, 574.32; Found, 574.99. Anal. Cacld for $C_{43}H_{42}O$: C, 89.85; H, 7.37; Found: C, 89.51; H, 7.20.

X2A. A white solid (2.53 g, 60%). ^{1}H NMR (400 MHz, $CDCl_3$) δ (ppm): 7.89 (s, 2H, ArH), 7.60 (s, 2H, ArH), 7.58 (s, 2H, ArH), 7.56 (d, *J* = 2.4 Hz, 2H, ArH), 7.04-6.96 (m, 5H, ArH), 6.75-6.71 (m, 5H, ArH), 1.90 (s, 6H, -CH_3), 1.30 (s, 18H, -CH_3). ^{13}C NMR (100 MHz, $CDCl_3$) δ (ppm): 146.22, 144.73, 132.12, 130.20, 129.24, 129.03, 127.87, 127.44, 125.90, 125.88, 125.37, 123.96, 123.89, 121.66, 35.17, 34.56, 32.61, 31.62. MS (EI, m/z): $[M]^+$calcd for: $C_{51}H_{46}O$, 674.35; Found, 674.18. Anal. Cacld for $C_{51}H_{46}O$: C, 90.76; H, 6.87; Found: C, 90.67; H, 7.08.

The cultivation of X2A crystals. 20 mg X2A was dissolved in 3 mL dichloromethane (CH_2Cl_2), dibromomethane (CH_2Br_2), and 1,2-dichloroethane ($ClCH_2CH_2Cl$), respectively, then solvent was evaporated at room temperature to acquire X2A-B-CH_2Cl_2 crystal, X2A-B-CH_2Br_2 crystal and X2A-B-$ClCH_2CH_2Cl$ crystal, respectively. 20 mg X2A was dissolved in 3 mL methyl iodide (CH_3I) and solvent was evaporated at low temperature (2-8 °C) to acquire X2A-B-CH_3I crystal. 20 mg X2A was dissolved in 3 mL tetrahydrofuran and solvent was evaporated at room temperature to acquire X2A-G crystal.

2 Additional data and spectra

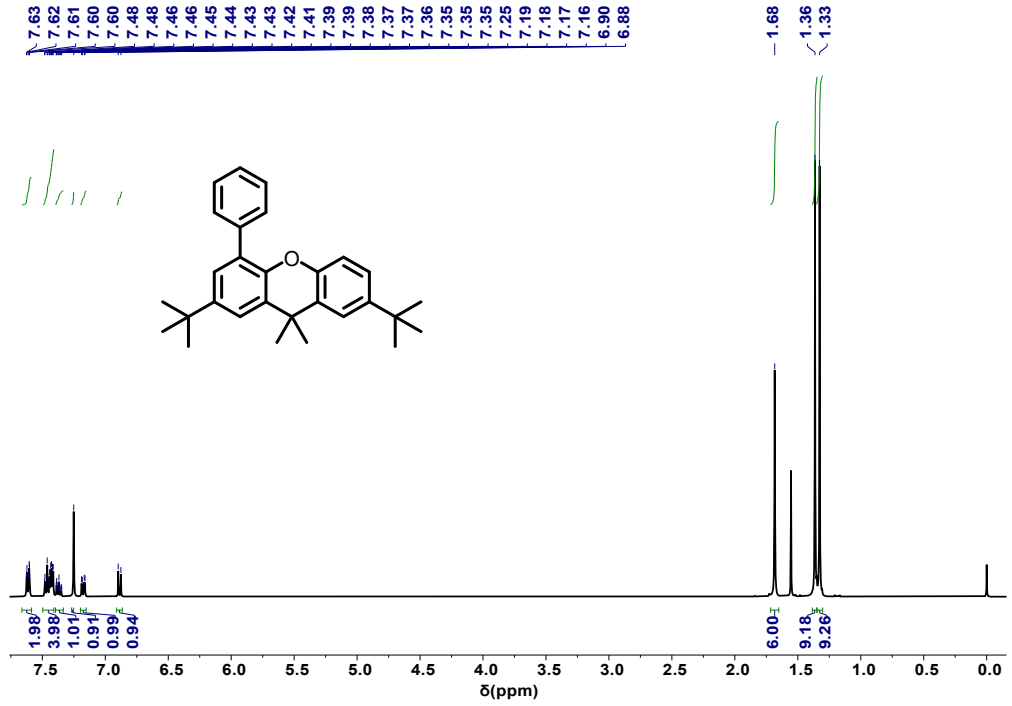

Fig. S1. ^{1}H NMR spectrum of X1B in $CDCl_3$ solution.

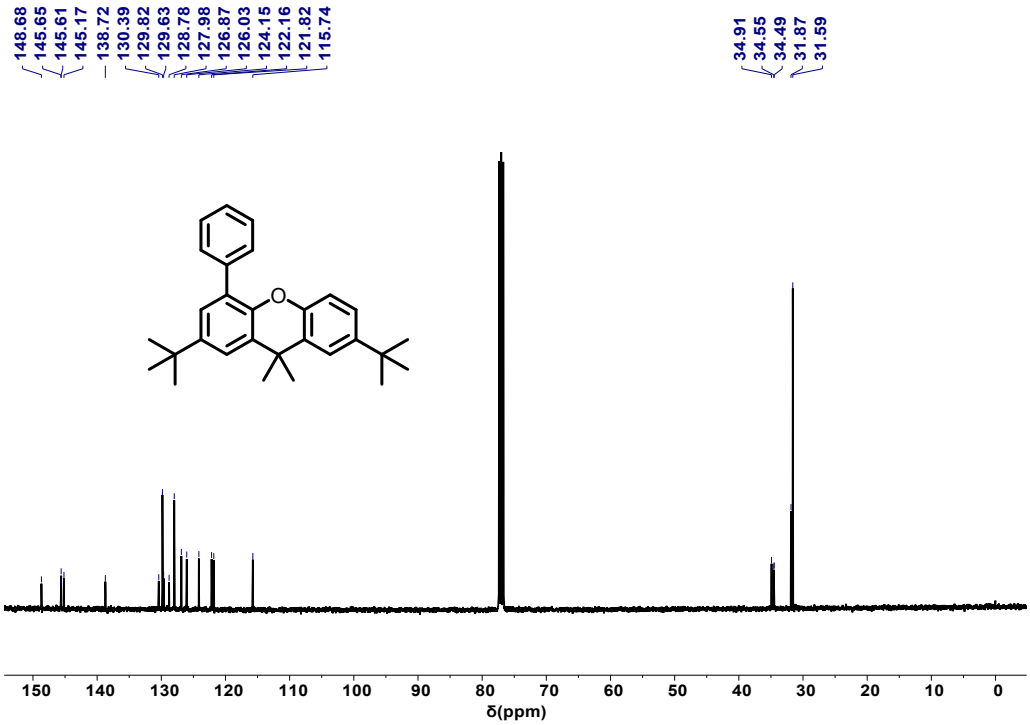

Fig. S2. ^{13}C NMR spectrum of X1B in $CDCl_3$ solution.

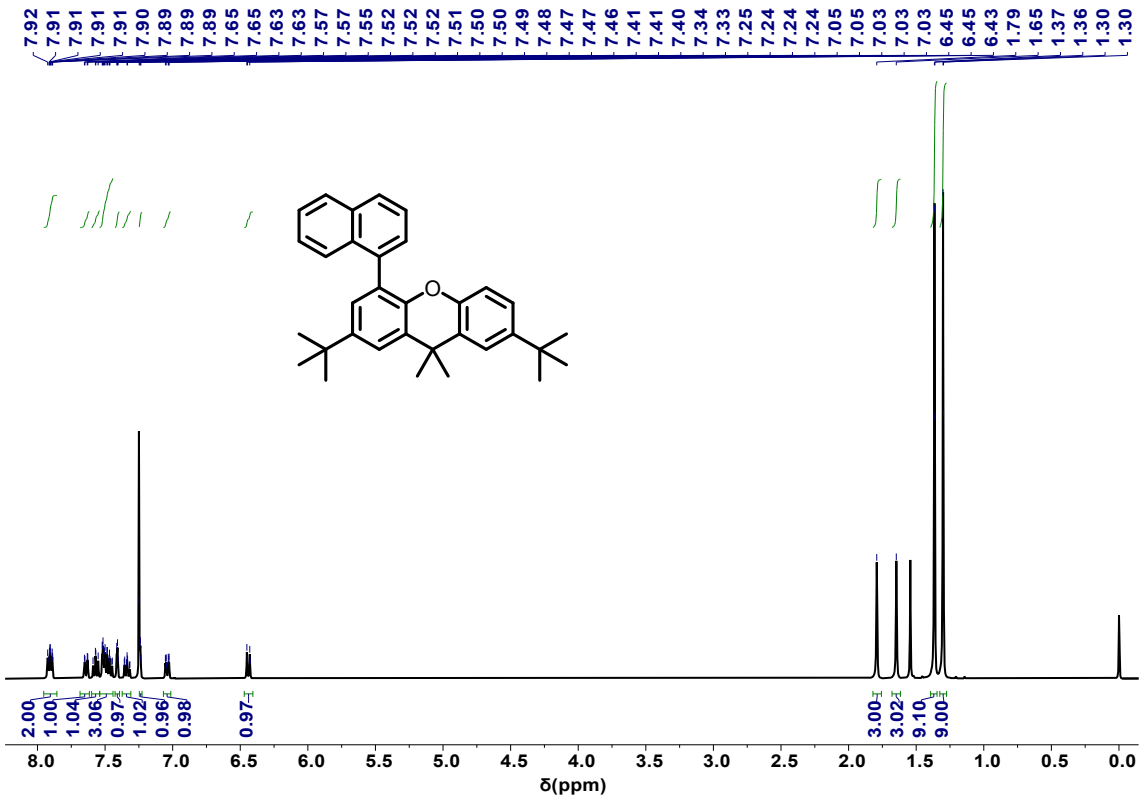

Fig. S3. ^{1}H NMR spectrum of X1N in $CDCl_3$ solution.

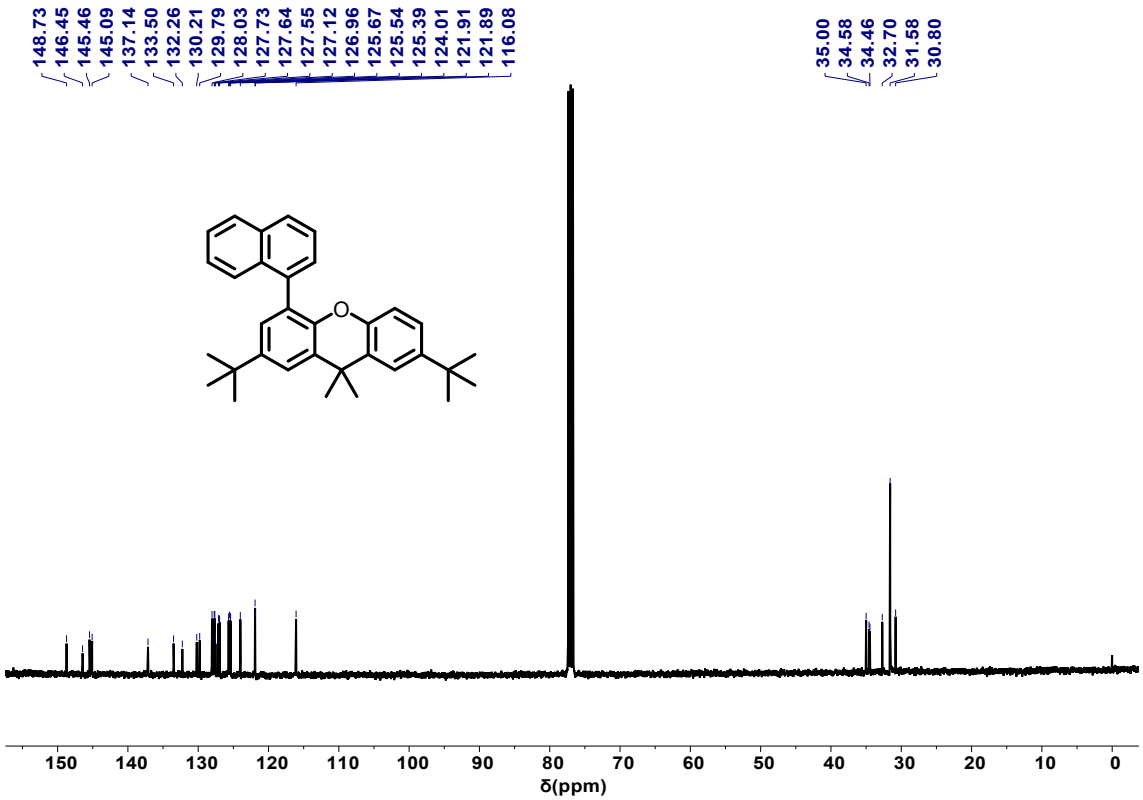

Fig. S4. ^{13}C NMR spectrum of X1N in $CDCl_3$ solution.

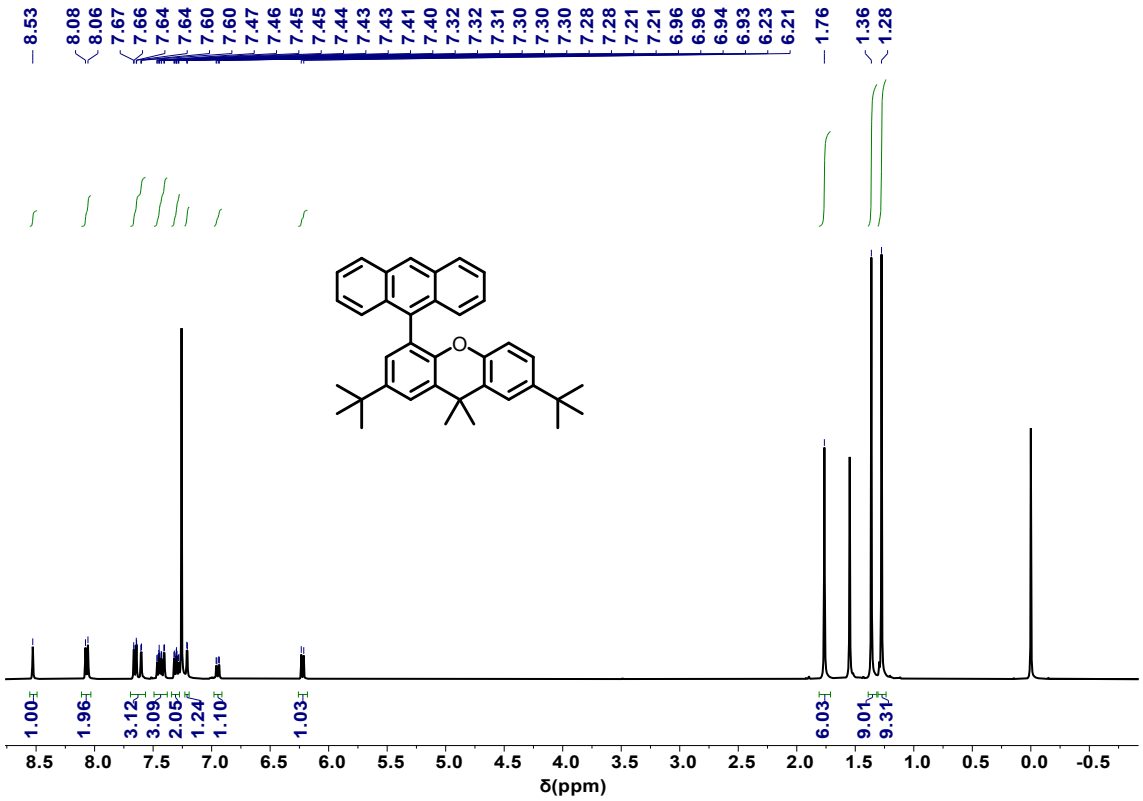

Fig. S5. ^{1}H NMR spectrum of X1A in $CDCl_3$ solution.

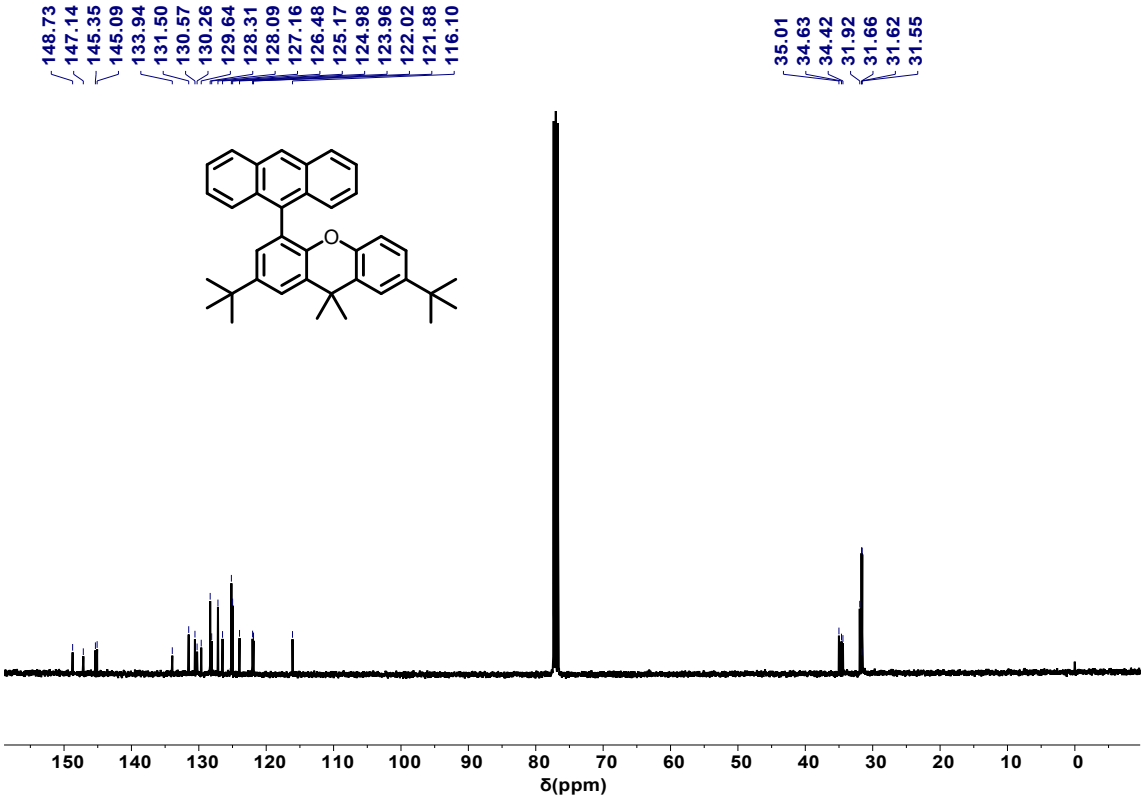

Fig. S6. ^{13}C NMR spectrum of X1A in $CDCl_3$ solution.

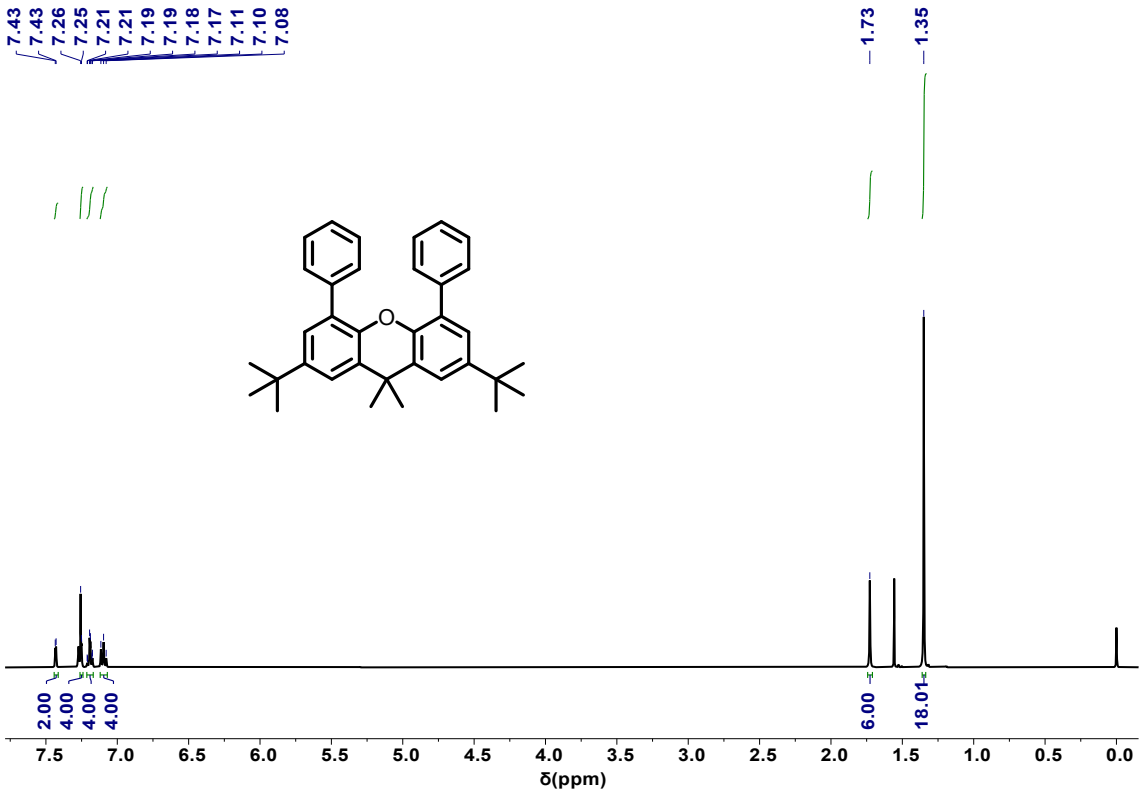

Fig. S7. ^{1}H NMR spectrum of X2B in $CDCl_3$ solution.

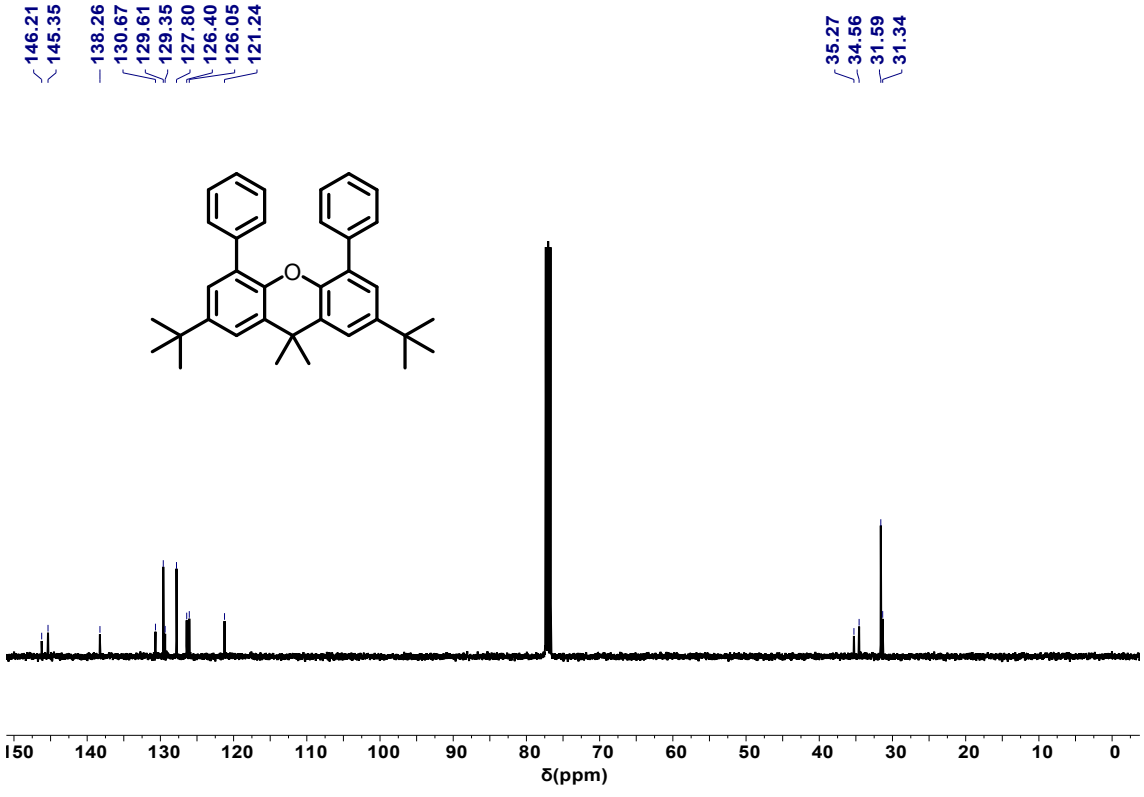

Fig. S8. ^{13}C NMR spectrum of X2B in $CDCl_3$ solution.

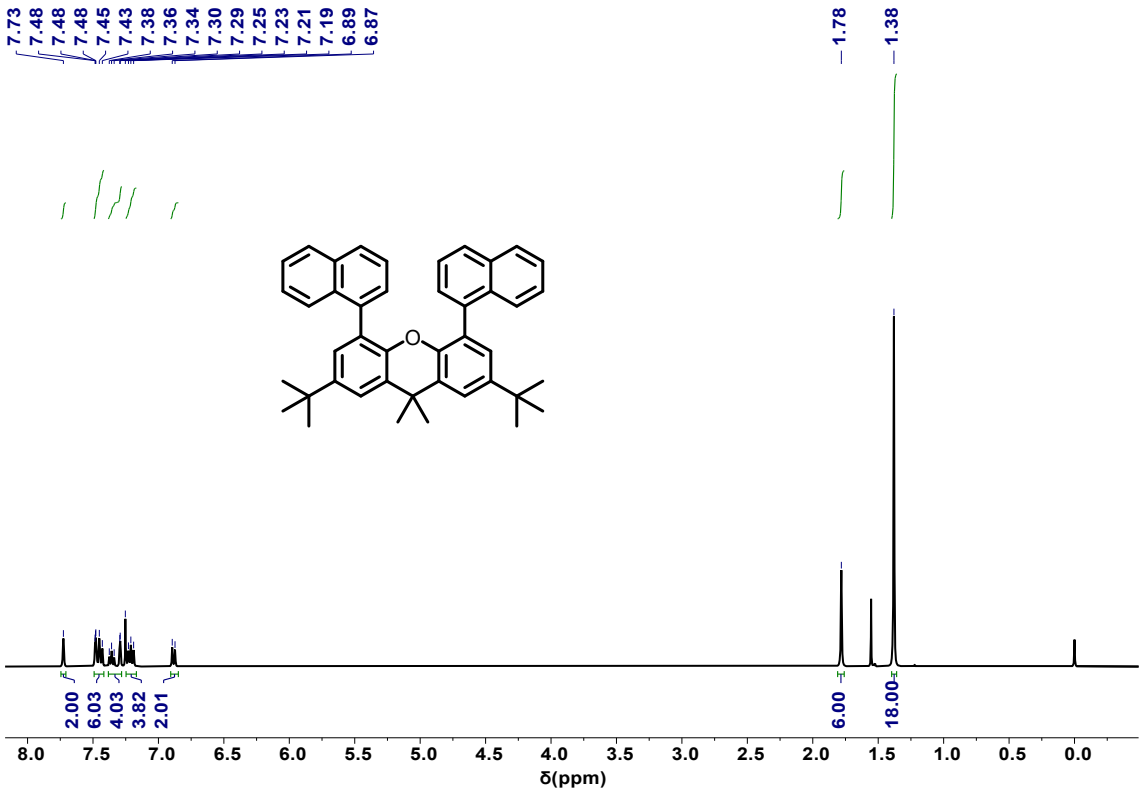

Fig. S9. ^{1}H NMR spectrum of X2N in $CDCl_3$ solution.

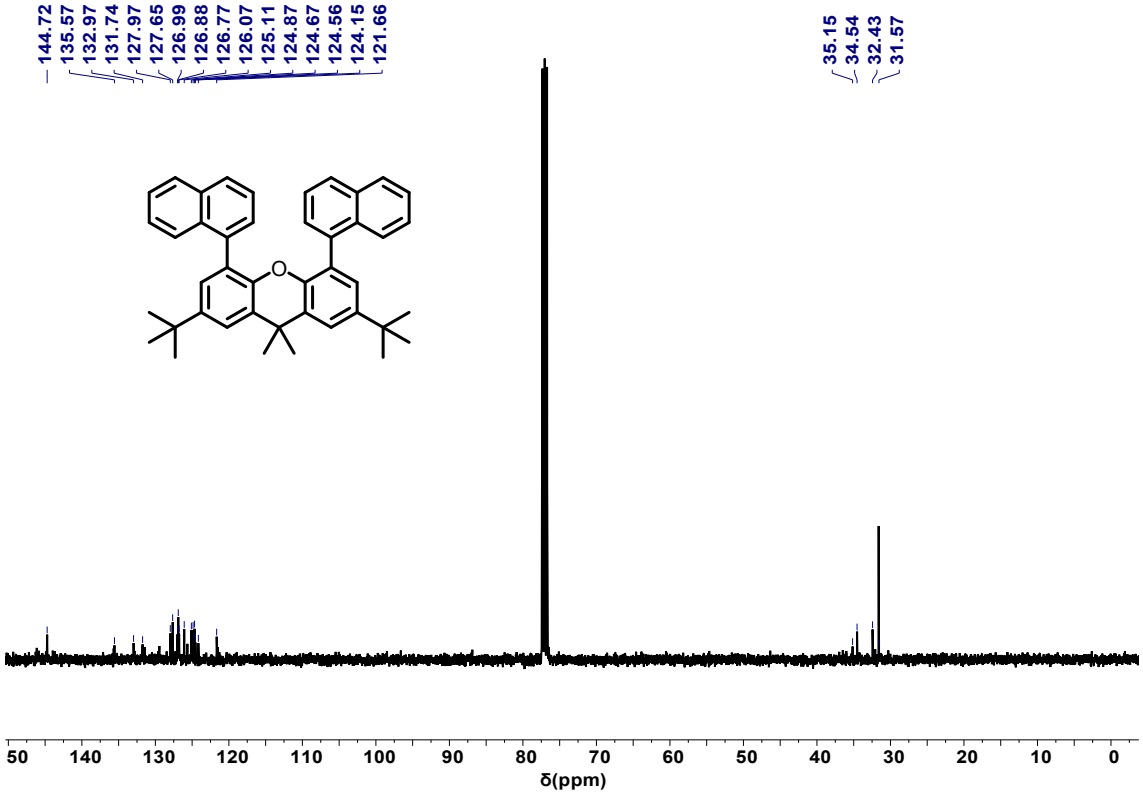

Fig. S10. ^{13}C NMR spectrum of X2N in $CDCl_3$ solution.

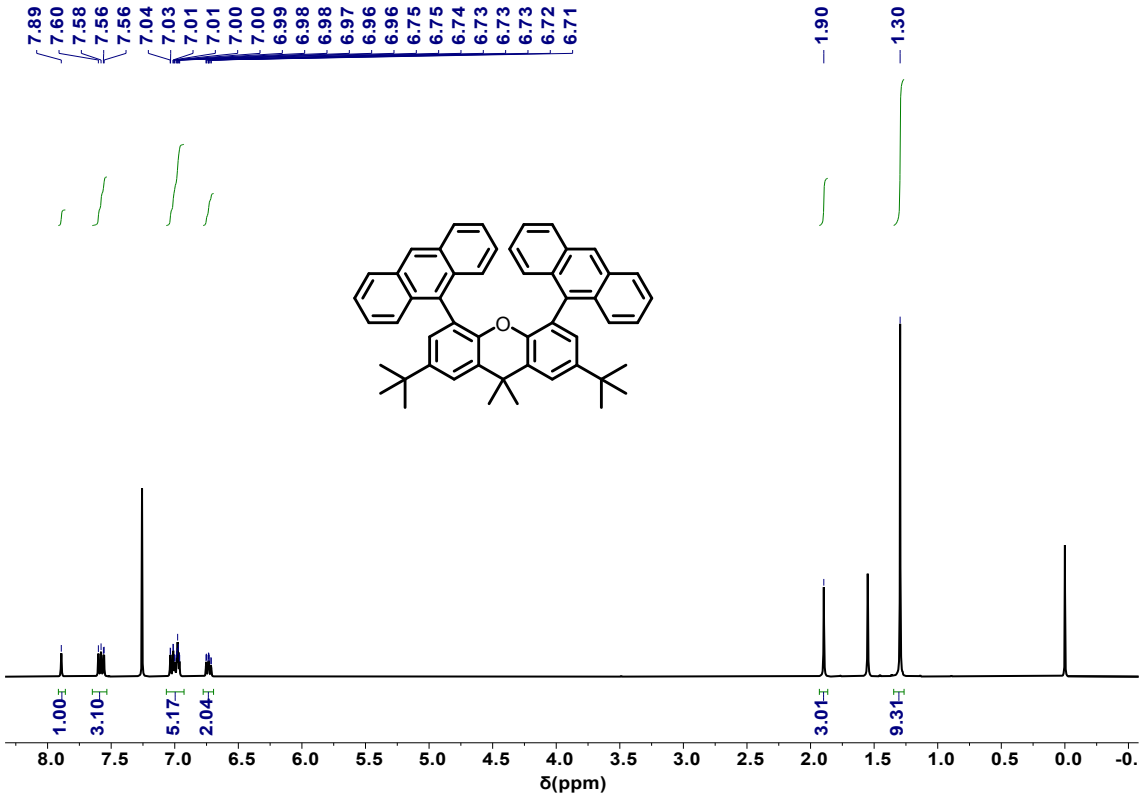

Fig. S11. ^{1}H NMR spectrum of X2A in $CDCl_3$ solution.

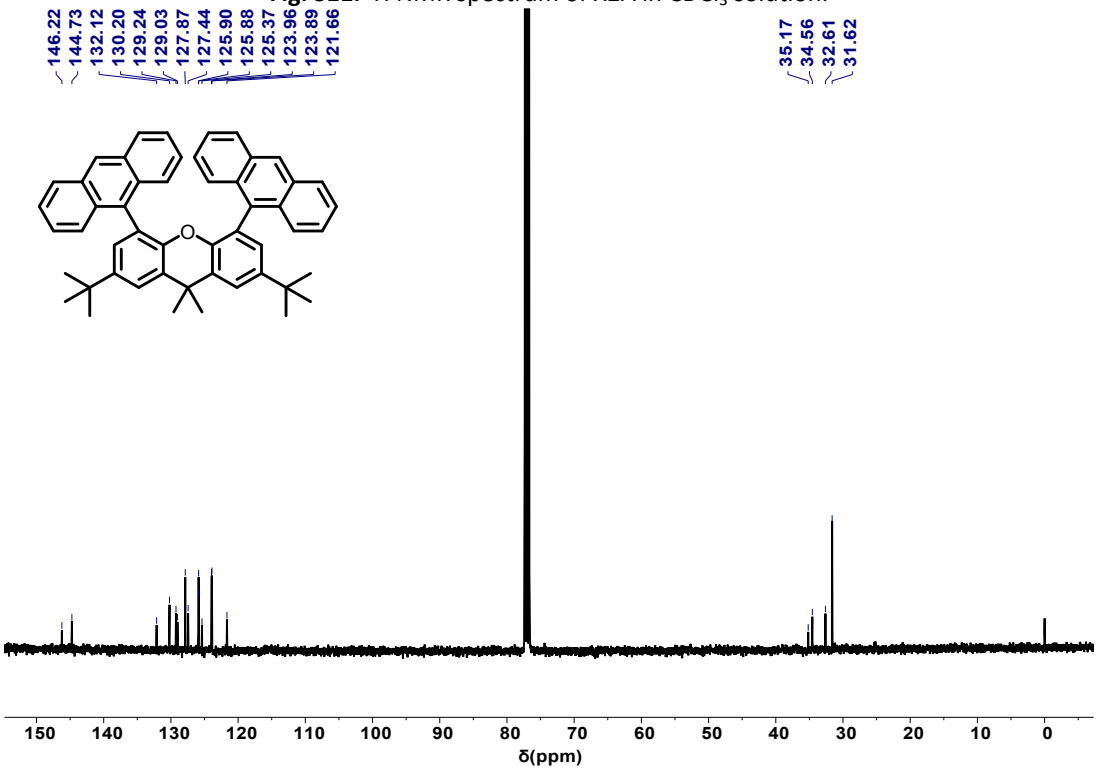

Fig. S12. ^{13}C NMR spectrum of X2A in $CDCl_3$ solution.

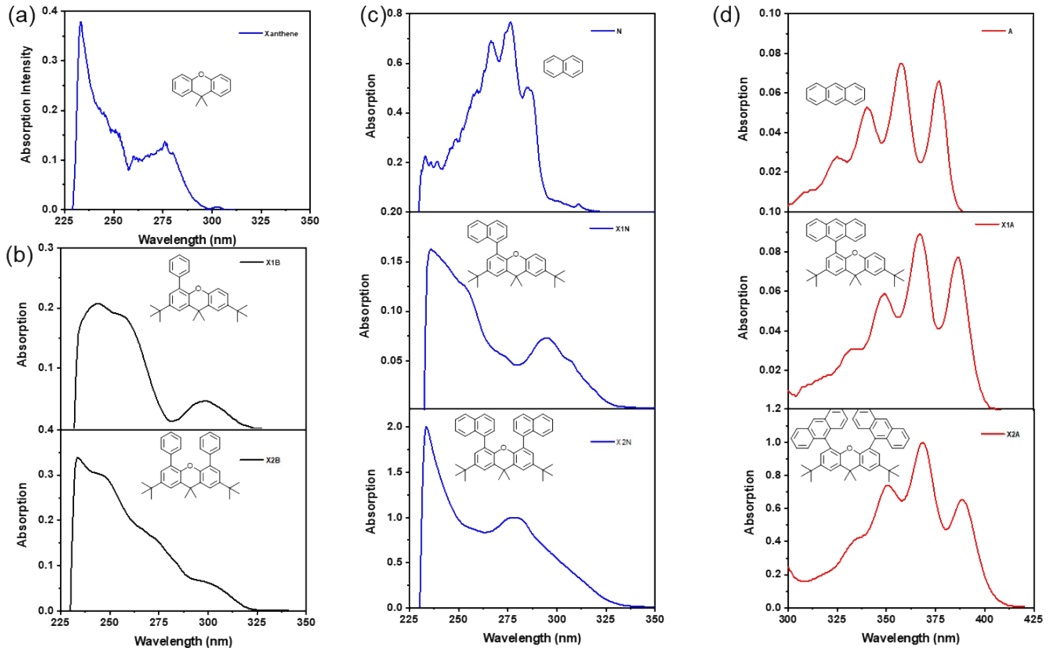

Fig. S13. Absorption spectra of (a) xanthene (b) X1B and X2B (c) naphthalene, X1N and X2N (d) anthracene, X1A and X2A in THF solution at room temperature. The concentration were all based on 10 μM THF solution except for naphthalene (100 μM), because the naphthalene solution with 10 μM showed weak absorption.

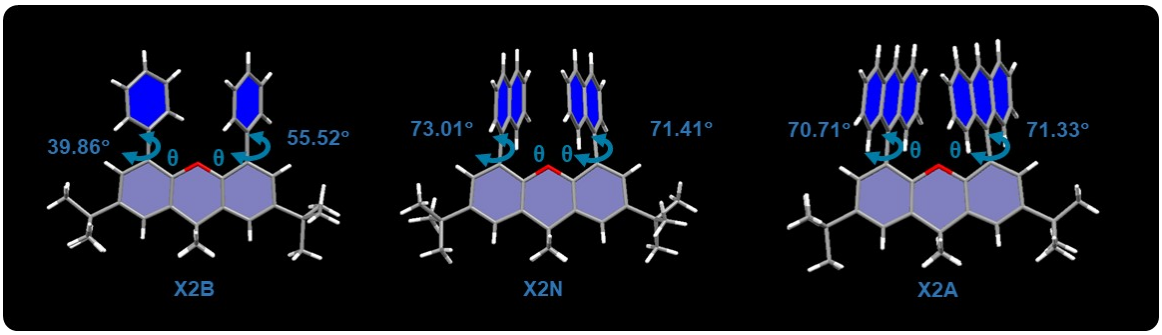

Fig. S14. Molecular geometry with dihedral angle between PAHs and xanthene scaffold in X2B, X2N and X2A crystal.

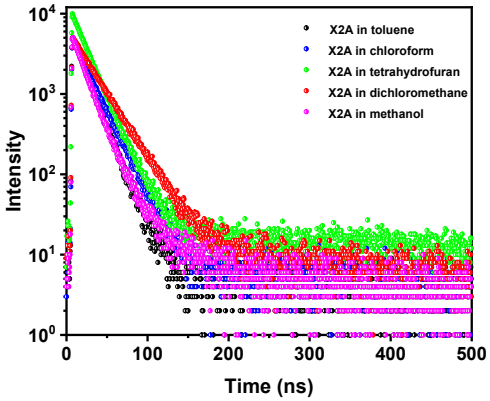

Compound	τ_F (ns)	PLQY (%)
Toluene	16.62	20.51%
Chloroform	20.40	28.41%
Tetrahydrofuran	18.29	24.91%
Dichloromethane	26.80	28.41%
Methanol	16.71	30.33%

Fig. S15. Fluorescence decay of X2A in different 10 μM solution (toluene, chloroform, tetrahydrofuran, dichloromethane, methanol) at room temperature with detailed fluorescence lifetime and PLQY.

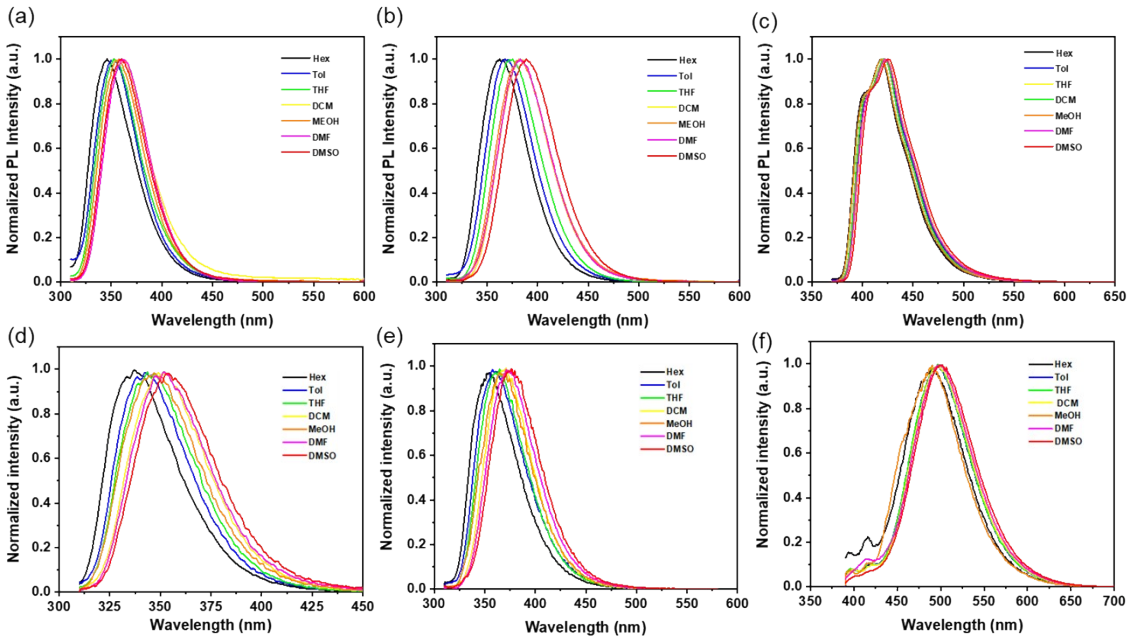

Fig. S16. Normalized PL spectra of (a) X1B (b) X1N (c) X1A (d) X2B (e) X2N (f) X2A in different solvents with different polarities at room temperature.

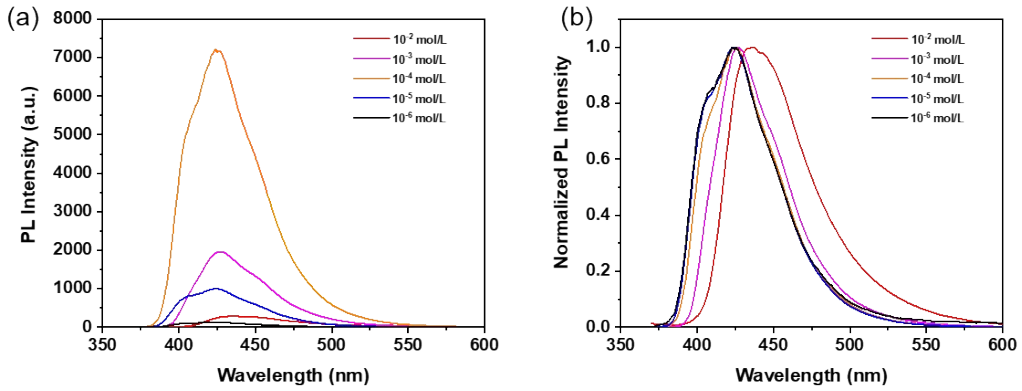

Fig. S17. (a) PL spectra and (b) Normalized PL spectra of X1A in THF solution with different concentration. (λ_{ex} =350 nm).

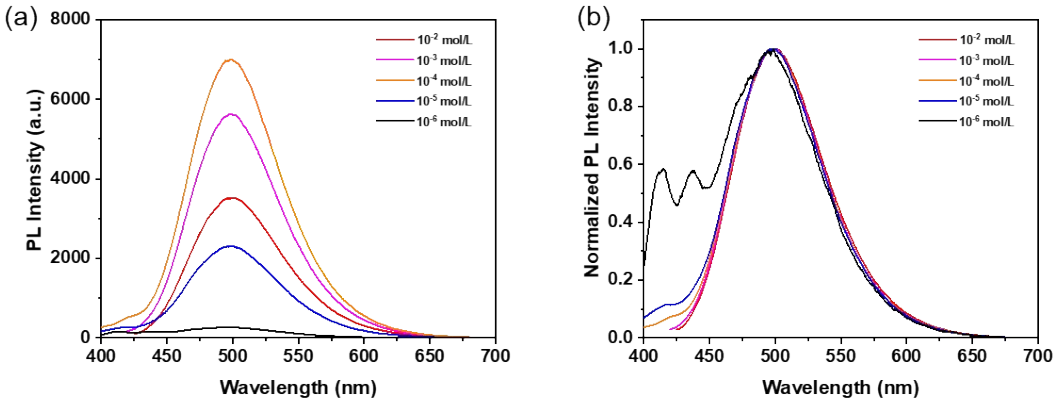

Fig. S18. (a) PL spectra and (b) Normalized PL spectra of X2A in THF solution with different concentration. (λ_{ex} =350 nm).

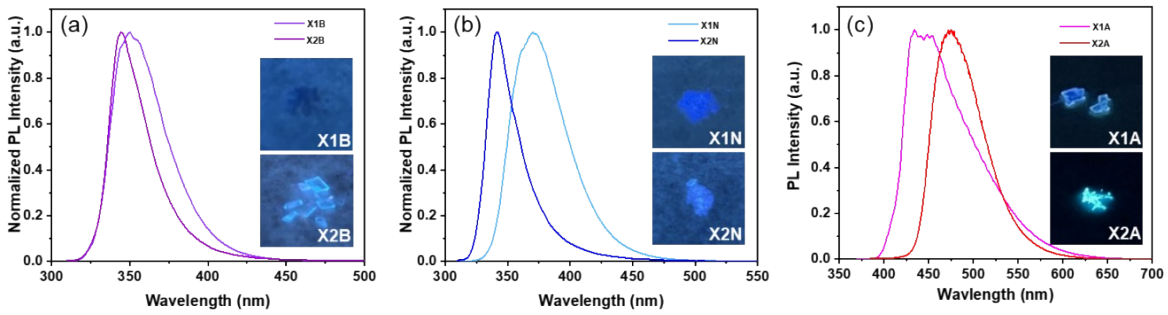

Fig. S19. PL spectra of (a) X1B and X2B, (b) X1N and X2N, (c) X1A and X2A crystals at room temperature. Insert were photographs of these crystals taken under 365 nm excitation.

Table S1. Photophysical properties of X1R and X2R derivatives at room temperature.

Compound	λ_{Abs}[a] (nm)	λ_F[a] (nm)	λ_F[b] (nm)
X1B	298	346	344
X2B	275, 299	353	352
X1N	295	375	378
X2N	280	365	361
Anthracene	340, 358, 377	385, 407, 427	432, 446
X1A	349, 367, 387	421	454
X2A	350, 369, 388	500	475

[a] In THF solution at concentration of 10 μM ; [b] Solid state.

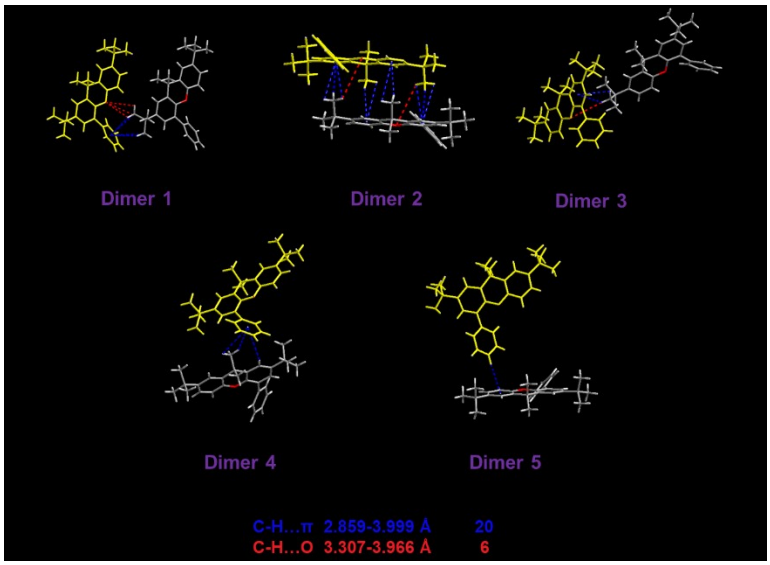

Fig. S20. Intermolecular interactions between one central molecule and adjacent molecules in X1B crystal.

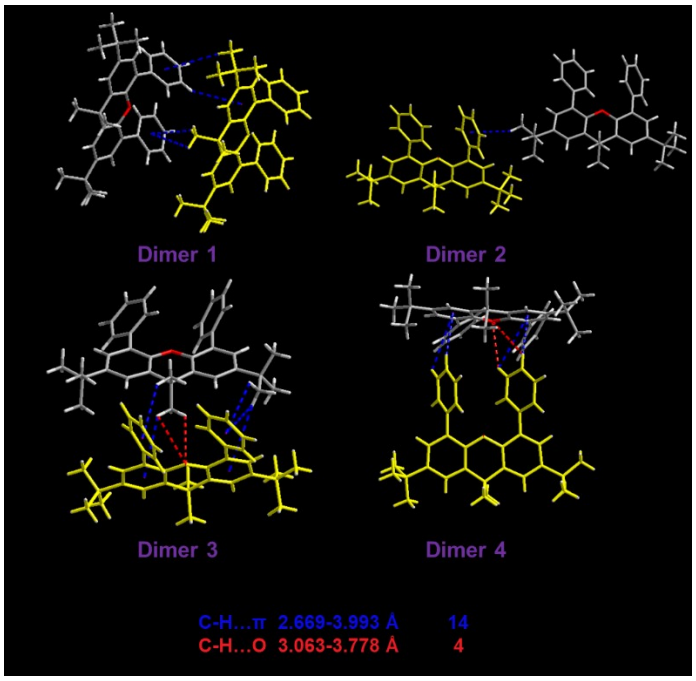

Fig. S21. Intermolecular interactions between one central molecule and adjacent molecules in X2B crystal.

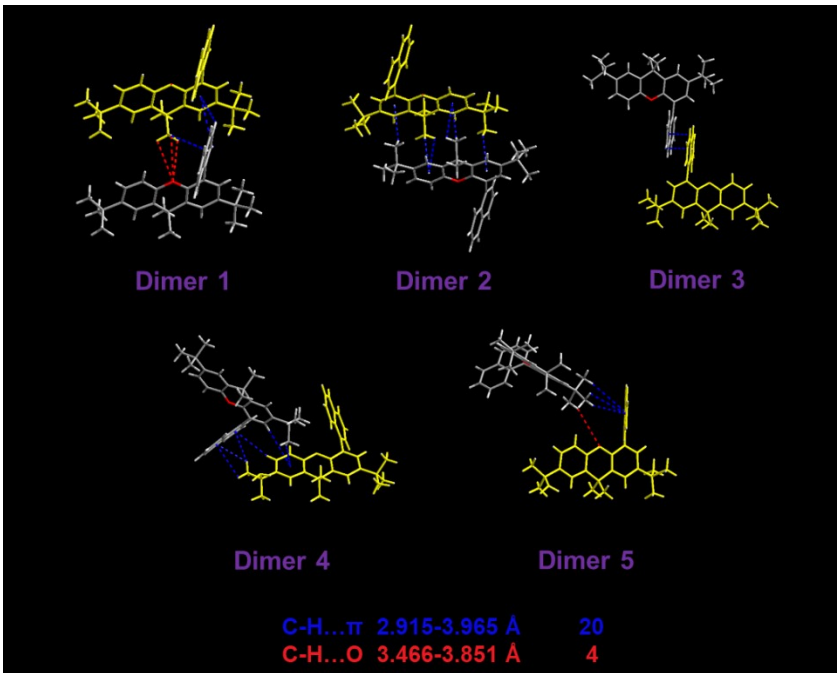

Fig. S22. Intermolecular interactions between one central molecule and adjacent molecules in X1N crystal.

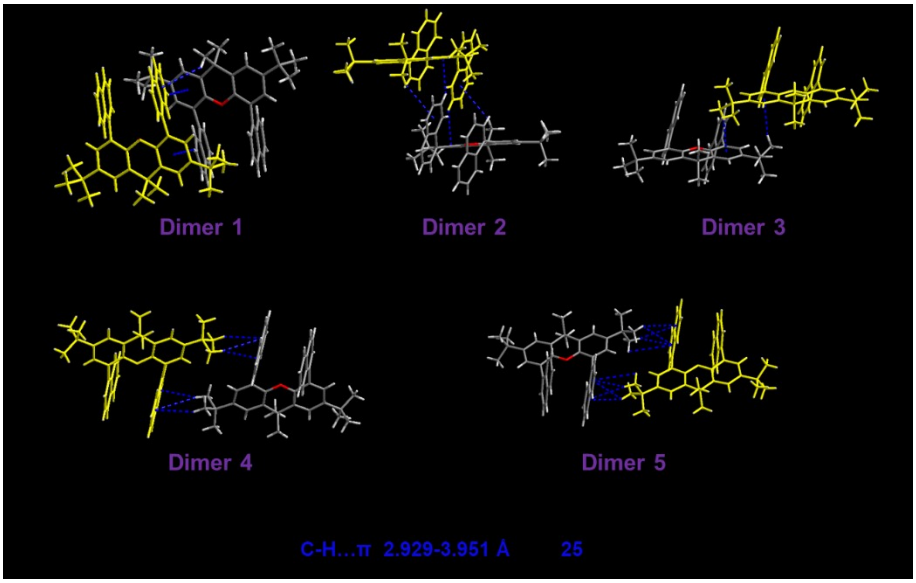

Fig. S23. Intermolecular interactions between one central molecule and adjacent molecules in X2N crystal.

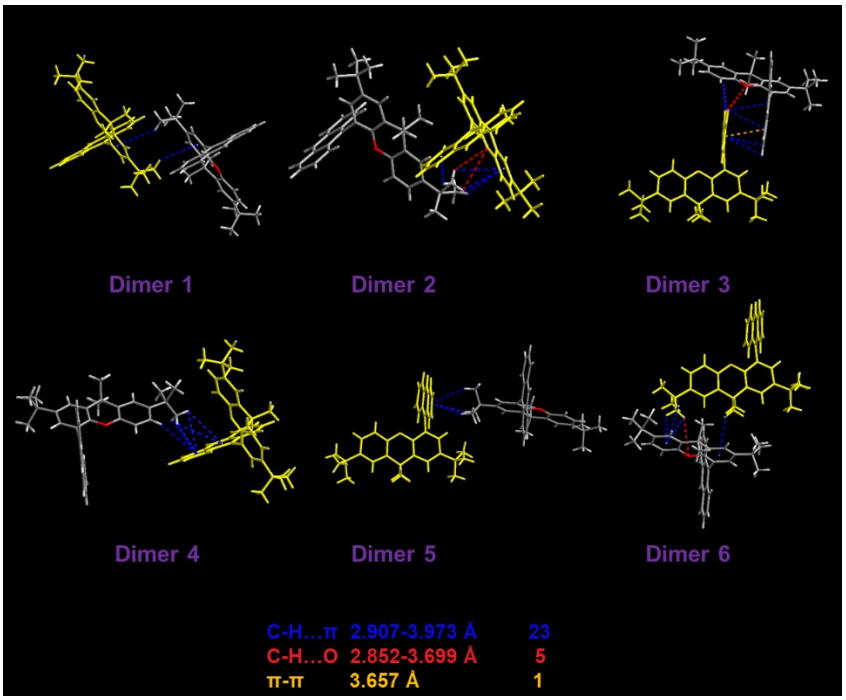

Fig. S24. Intermolecular interactions between one central molecule and adjacent molecules in X1A crystal.

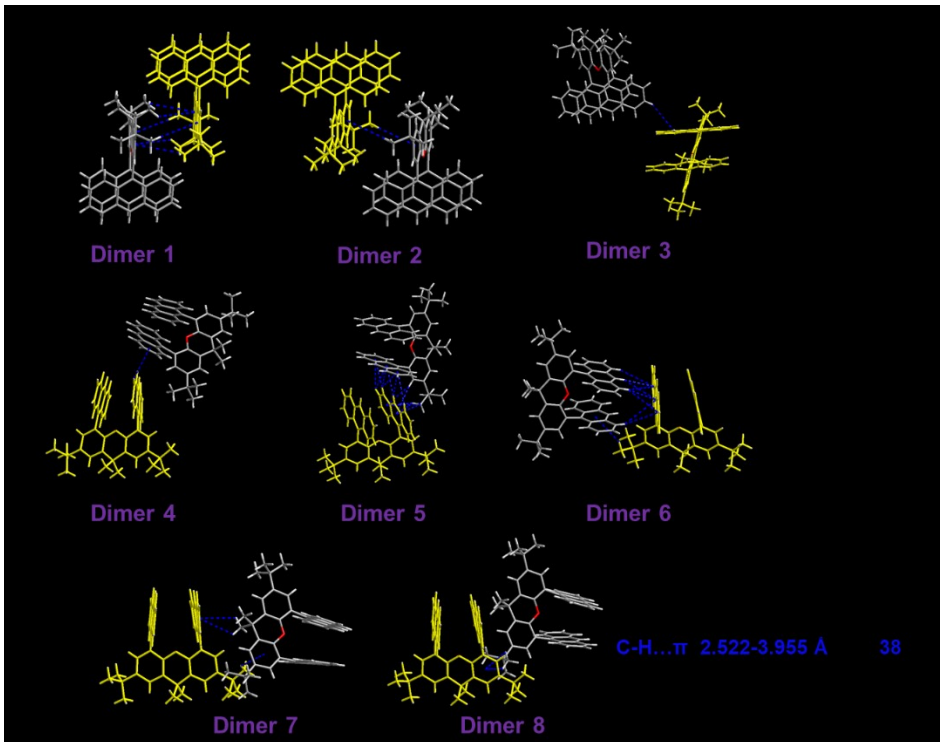

Fig. S25. Intermolecular interactions between one central molecule and adjacent molecules in X2A-G crystal.

Table S2. Structural data of single crystals based on X1R and X2R derivatives.

Name	X1B	X2B	X1N	X2N	X1A	X2A-G
Formula	C_{29} H_{34} O	C_{35} H_{38} O	C_{33} H_{36} O	C_{43} H_{42} O	C_{37} H_{38} O	C_{51} H_{46} O
Wavelength (Å)	0.71073	0.71073	0.71073	0.71073	0.71073	0.71073
Space Group	P 21/c	P 21/n	P 21/c	P -1	P bca	P -1
Cell Lengths (Å)	a = 9.2535 (18) b = 14.900 (3) c = 17.885 (4)	a = 8.6293 (12) b = 12.4614 (17) c = 26.146 (4)	a = 7.2553 (15) b = 20.450 (4) c = 18.243 (4)	a = 9.3608 (17) b = 14.084 (3) c = 14.199 (3)	a = 13.254 (3) b = 11.5590 (16) c = 38.103 (5)	a = 11.3817 (17) b = 18.157 (3) c = 19.306 (3)
Cell Angles (°)	α= 90° β= 101.861 (4)° γ= 90°	α= 90° β= 94.519 (2)° γ= 90°	α= 90° β= 100.989 (4)° γ= 90°	α= 66.933 (3)° β= 81.559 (3)° γ= 75.738 (3)°	α= 90° β= 90° γ= 90°	α= 83.855 (2)° β= 81.230 (2)° γ= 81.719 (2)°
Cell Volume ($Å^3$)	2413.2 (8)	2802.8 (7)	2657.2 (10)	1666.6 (5)	5837.6 (18)	3887.2 (11)
Z	4	4	4	2	8	4
Density (g/cm^3)	1.097	1.125	1.121	1.145	1.135	1.153
F (000)	864.0	1024.0	968.0	616.0	2144.9	1440.6
h_{max}, k_{max}, l_{max}	11, 17, 21	10, 15, 32	10, 28, 25	11, 18, 18	15, 13, 45	13, 21, 23
CCDC Number	2180328	2180349	2180336	2180351	2180337	2180353

Table S3. Intermolecular interactions of X1R and X2R crystals at room temperature.

Compound	C-H…π	number	C-H…O	number	π-π	number
X1B	2.859-3.999 Å	20	3.307-3.966 Å	6	--	--
X2B	2.669-3.993 Å	14	3.063-3.778 Å	4	--	--
X1N	2.915-3.965 Å	20	3.466-3.851 Å	4	--	--
X2N	2.929-3.951 Å	25	--	--	--	--
X1A	2.907-3.973 Å	23	2.852-3.699 Å	5	3.657 Å	1
X2A-G	2.522-3.955 Å	38	--	--	--	--

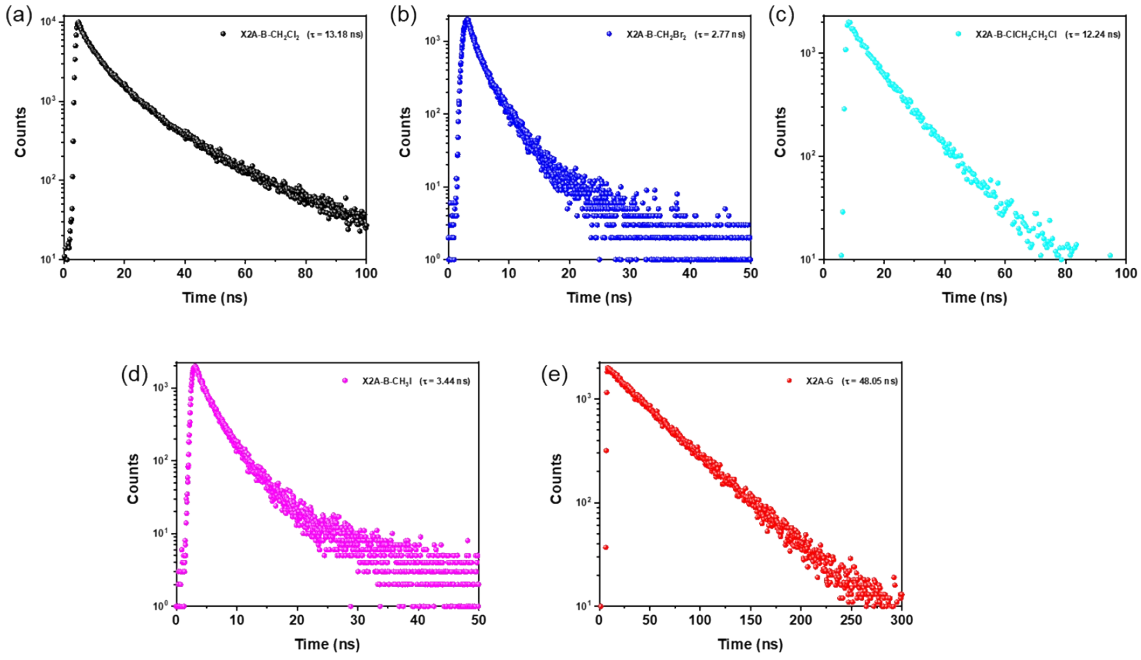

Fig. S26. Fluorescence decay of (a) X2A-B-CH_2Cl_2, (b) X2A-B-CH_2Br_2, (c) X2A-B-$ClCH_2CH_2Cl$, (d) X2A-B-CH_3I and (e) X2A-G crystals at room temperature.

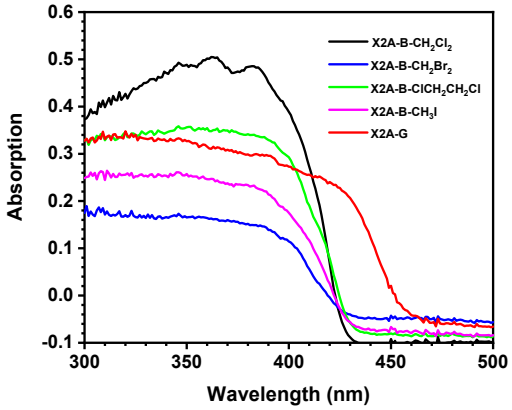

Fig. S27. Absorption spectra of X2A crystals (X2A-B-CH_2Cl_2, X2A-B-CH_2Br_2, X2A-B-$ClCH_2CH_2Cl$, X2A-B-CH_3I, X2A-G).

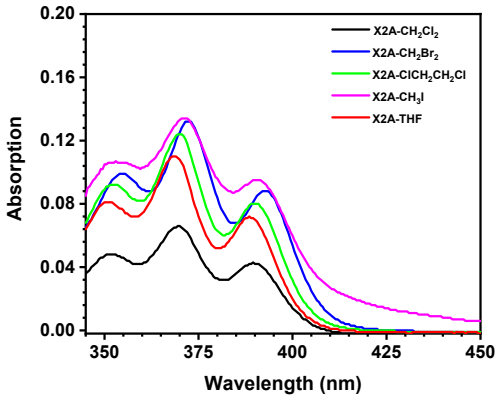

Fig. S28. Absorption spectra of X2A compound in CH_2Cl_2 solution, CH_2Br_2 solution, $ClCH_2CH_2Cl$ solution, CH_3I solution and THF solution (10 μM).

Table S4. Photophysical properties of X2A crystals at room temperature.

Crystal	λ_{Abs}[a] (nm)	λ_F[a] (nm)	λ_{Abs}[b] (nm)	λ_F[b] (nm)	τ_F[b] (ns)	Φ_{PL}[b] (%)	CCDC number
X2A-B-CH_2Cl_2	351, 370, 390	505	300~431	432, 447	13.18	45.57	2180355
X2A-B-CH_2Br_2	354, 371, 392	511	300~433	430, 450	2.77	4.42	2180357
X2A-B-$ClCH_2CH_2Cl$	351, 369, 389	506	300~433	435, 448	12.24	54.69	2180359
X2A-B-CH_3I	353, 370, 390	508	300~434	432, 451	3.44	16.03	2180360
X2A-G	350, 368, 389	504	300~465	481	48.05	~100	2180353

[a] In solution at concentration of 10 μM; X2A-B-CH_2Cl_2 in dichloromethane, X2A-B-CH_2Br_2 in dibromomethane, X2A-B-$ClCH_2CH_2Cl$ in 1,2-dichloroethane, X2A-B-CH_3I in methyl iodide, X2A-G in tetrahydrofuran. [b] Crystal.

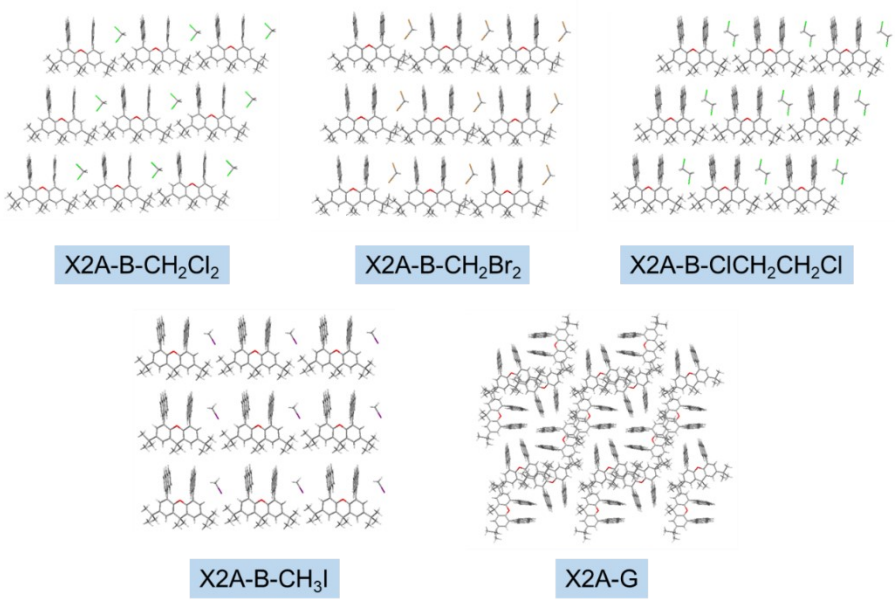

Fig. S29. Molecular packing modes of polymorphs of X2A-B-CH_2Cl_2 crystal, X2A-B-CH_2Br_2 crystal, X2A-B-$ClCH_2CH_2Cl$ crystal, X2A-B-CH_3I crystal, X2A-G crystal.

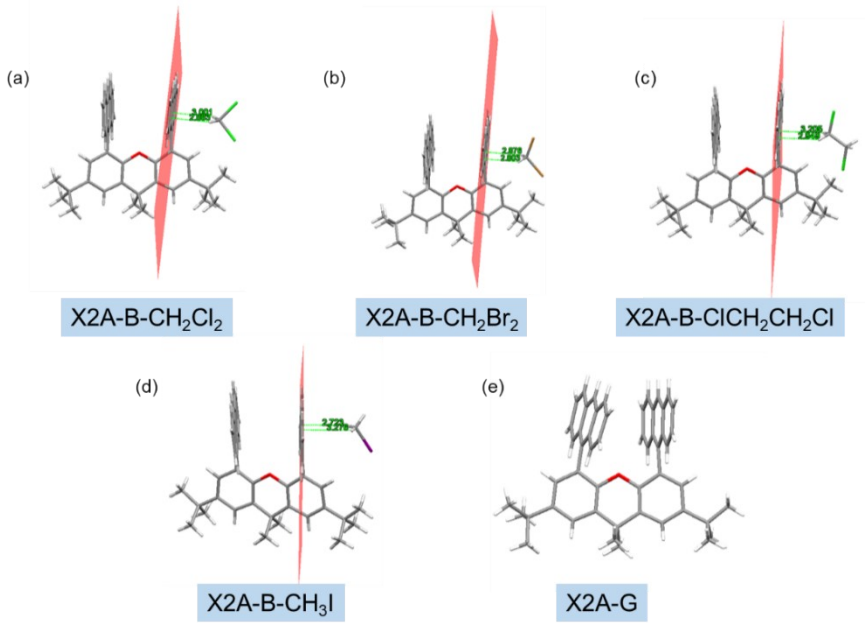

Fig. S30. Single crystal structures and intermolecular interactions between X2A molecule and solvent molecules of (a) X2A-B-CH_2Cl_2, (b) X2A-B-CH_2Br_2, (c) X2A-B-$ClCH_2CH_2Cl$, (d) X2A-B-CH_3I and (e) X2A-G.

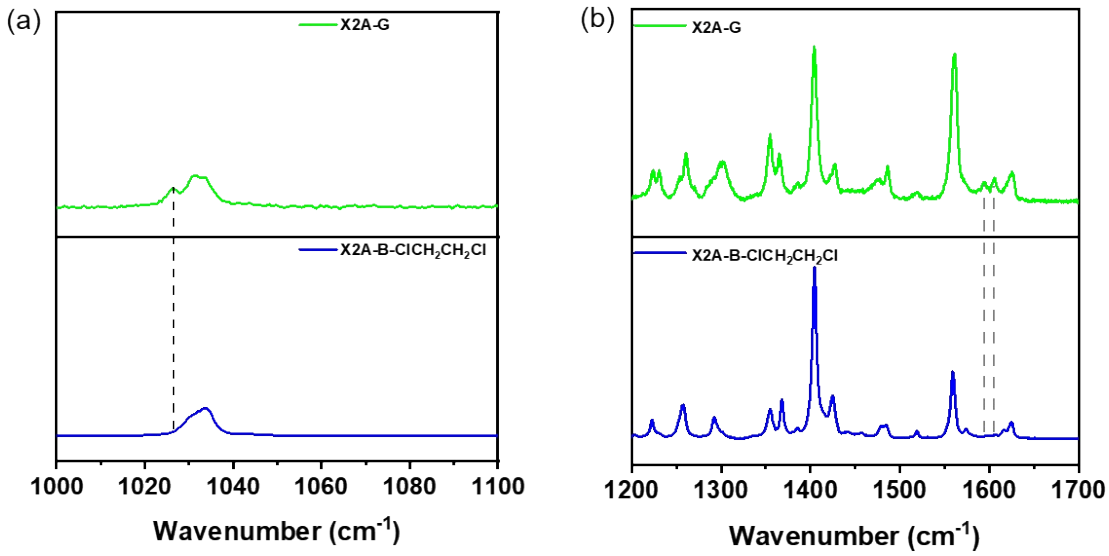

Fig. S31. Raman spectra of X2A-B-$ClCH_2CH_2Cl$ and X2A-G crystals with a laser at (a) 633 nm and (b) 785 nm.

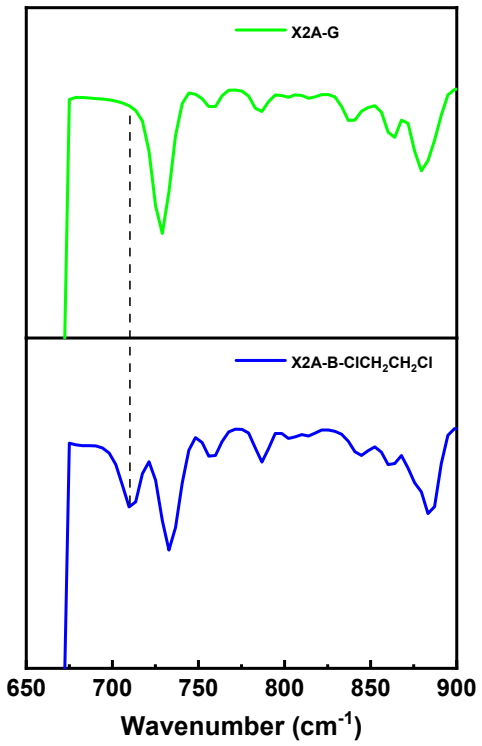

Fig. S32. Micro-infrared spectra of X2A-B-$ClCH_2CH_2Cl$ and X2A-G crystal at room temperature.

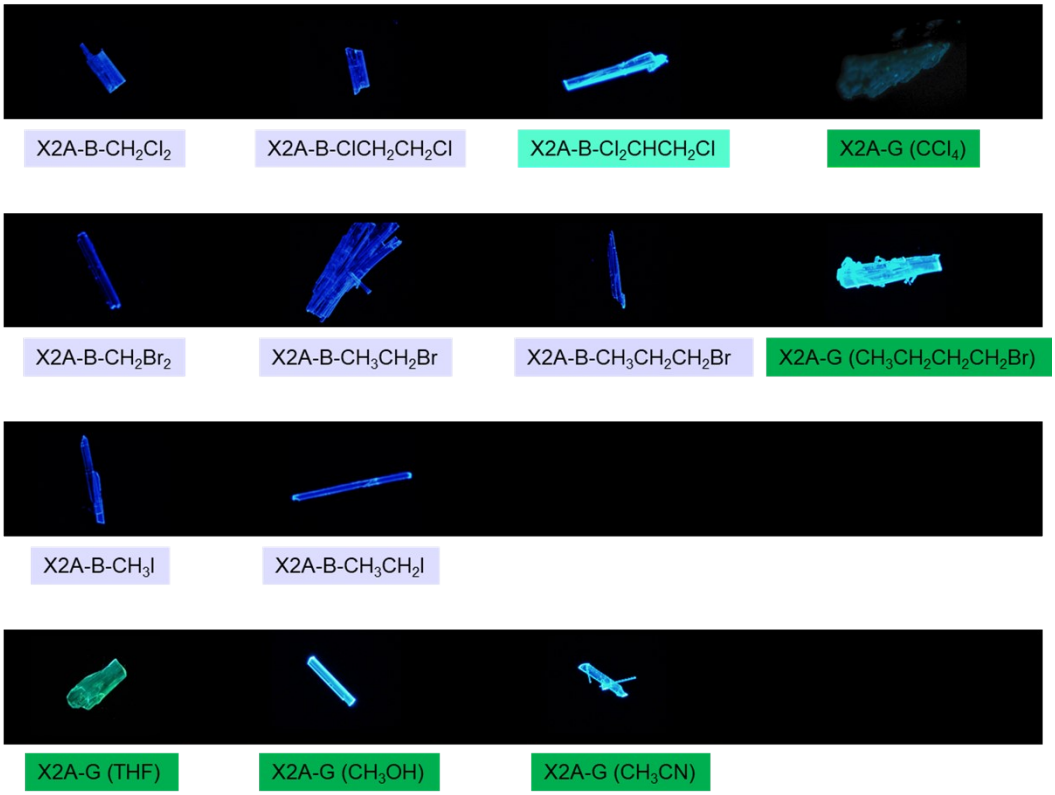

Fig. 33. Emission images of X2A crystals cultivated from different solvents.

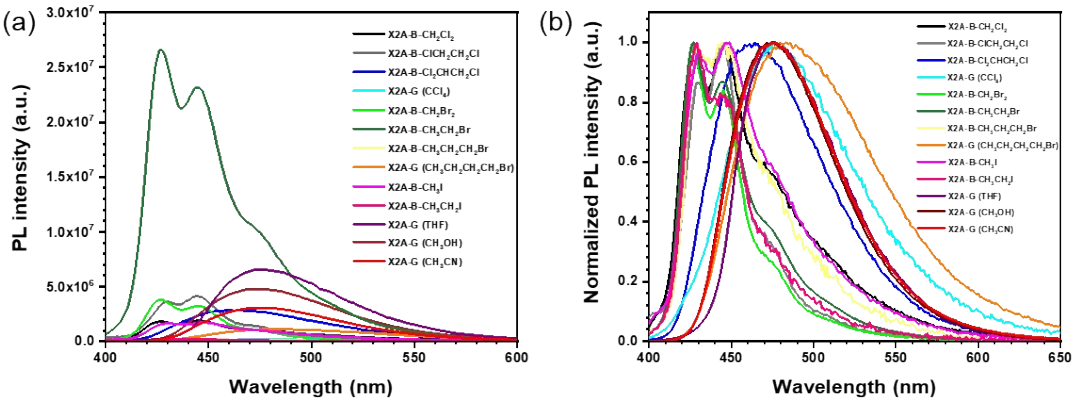

Fig. 34. (a) PL spectra and (b) Normalized PL spectra of X2A crystals cultivated from different solvents.

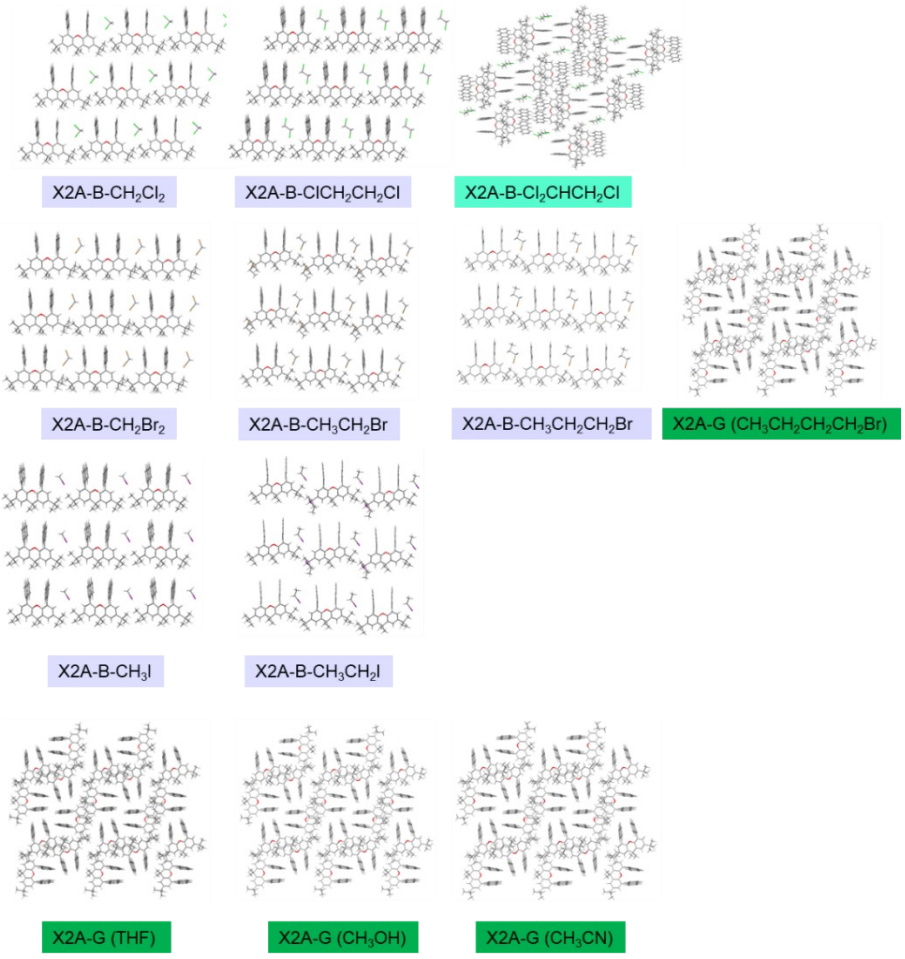

Fig. 35. Crystal structure of X2A crystals cultivated from different solvents (the quality of crystal cultivated from CCl_4 is bad for obtaining crystal structure).

Table S5. CCDC numbers of X2A crystals.

Name	CCDC Number
X2A-B-Cl_2CHCH_2Cl	2308124
X2A-B-CH_3CH_2Br	2308125
X2A-B-$CH_3CH_2CH_2Br$	2308126
X2A-G ($CH_3CH_2CH_2CH_2Br$)	2308127
X2A-CH_3CH_2I	2308248
X2A-G (CH_3OH)	2308129
X2A-G (CH_3CN)	2308128

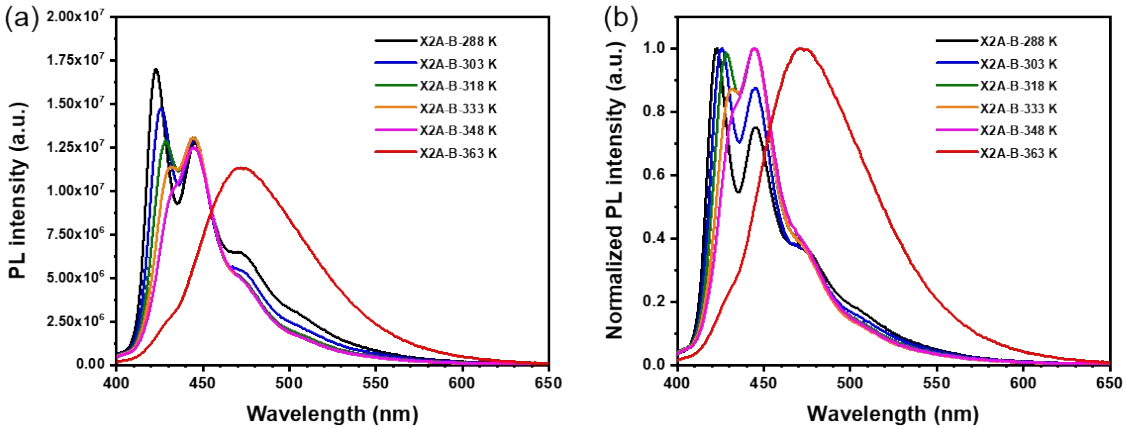

Fig. S36. (a) PL spectra and (b) Normalized PL spectra of X2A-B-$ClCH_2CH_2Cl$ crystal with temperature increasing from 288 K to 363 K.

Table S6. The maximum emission wavelength of X2A-B-$ClCH_2CH_2Cl$ crystal with temperature increasing from 288 K to 363 K.

Temperature / K	288	303	318	333	348	363
Emission wavelength (nm)	428	426	428	431	432	
	445	445	445	445	445	474
	470	470	472	473	473	

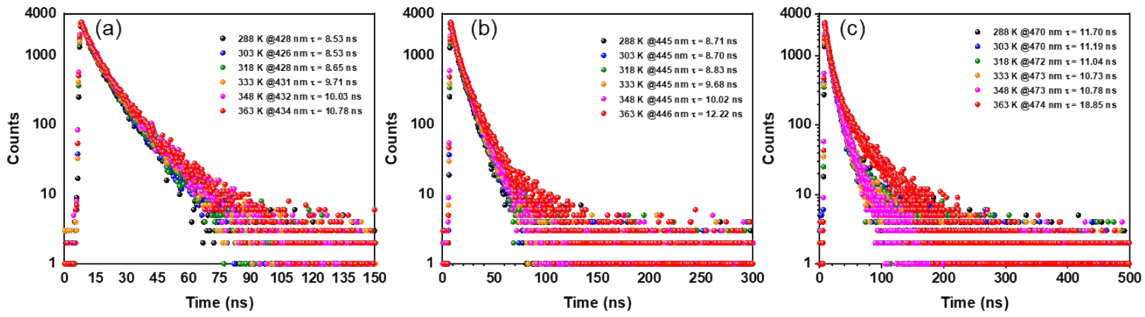

Fig. S37. Fluorescence decay of X2A-B-$ClCH_2CH_2Cl$ crystal with the temperature increasing from 288 K to 363 K at (a) 426-434 nm, (b) 445-446 nm, (c) 470-474 nm.

Table S7. Summary data of fluorescence lifetime of X2A-B-$ClCH_2CH_2Cl$ crystal with temperature increasing from 288 K to 363 K at 426-434 nm, (b) 445-446 nm, (c) 470-474 nm.

Temperature / K	288	303	318	333	348	363
$\tau_{426\text{-}434\ nm}$ (ns)	8.53	8.53	8.65	9.71	10.03	10.78
$\tau_{445\text{-}446\ nm}$ (ns)	8.71	8.70	8.83	9.68	10.02	12.22
$\tau_{470\text{-}474\ nm}$ (ns)	11.70	11.19	11.04	10.73	10.78	18.85

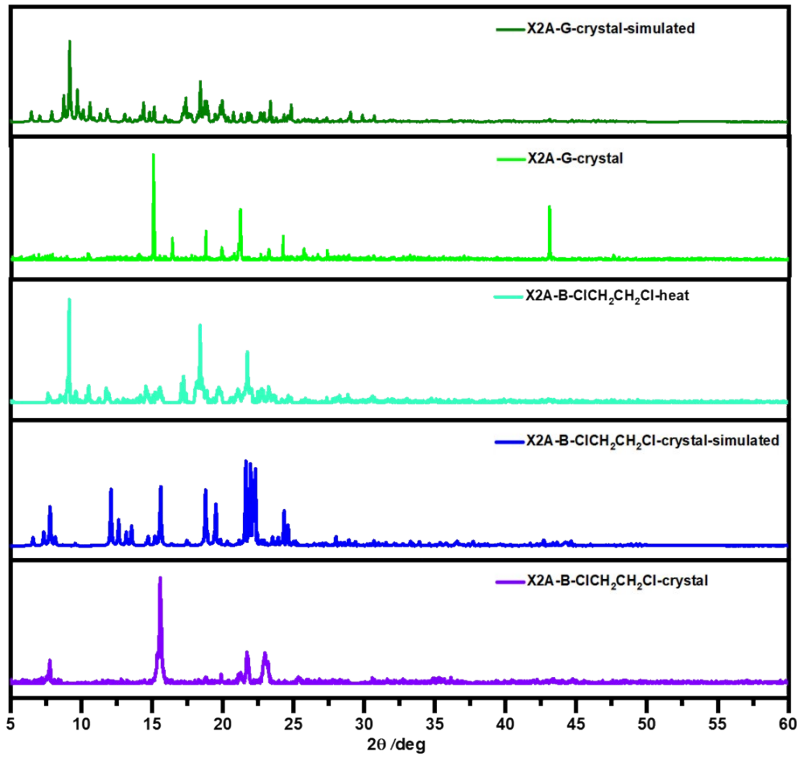

Fig. S38. PXRD patterns of X2A-B-$ClCH_2CH_2Cl$ crystal before and after heat, and X2A-G crystal.

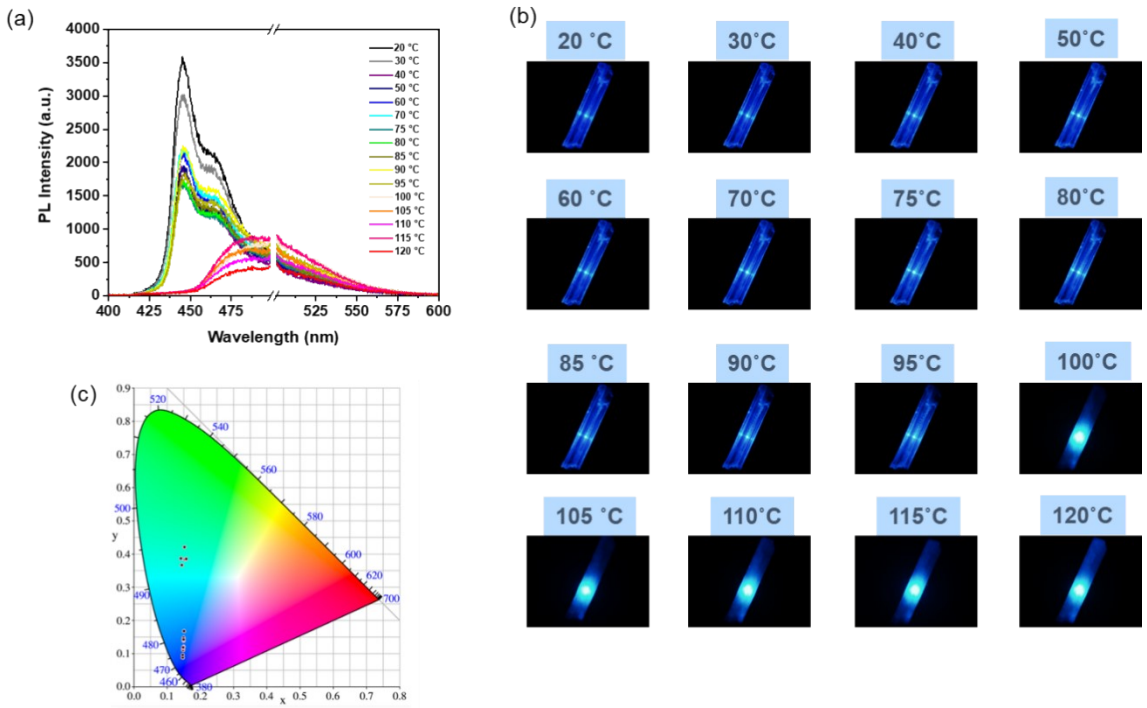

Fig. S39. (a) PL spectra and (b) fluorescence emission images of X2A-B-CH_2Cl_2 crystal at different temperature. (c) CIE coordinate of X2A-B-CH_2Cl_2 crystal at different temperature.

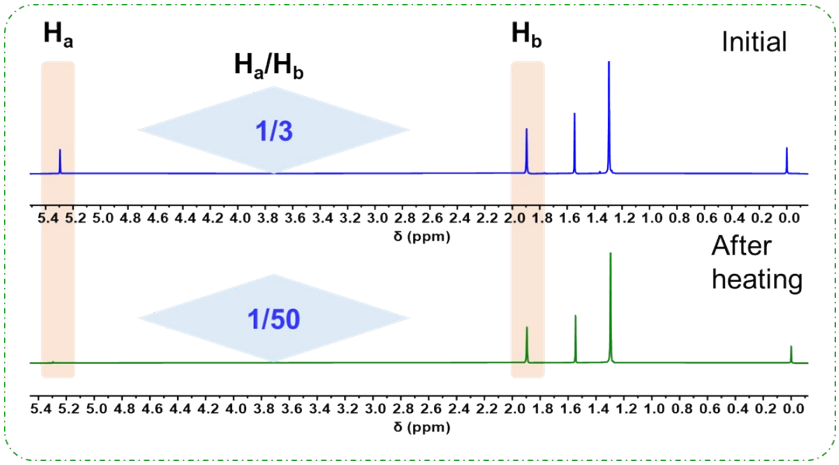

Fig. S40. ^1H NMR spectra of X2A-B-CH_2Cl_2 crystal in $CDCl_3$ at initial state or after heating at 363 K (with the ratio of H_a and H_b).

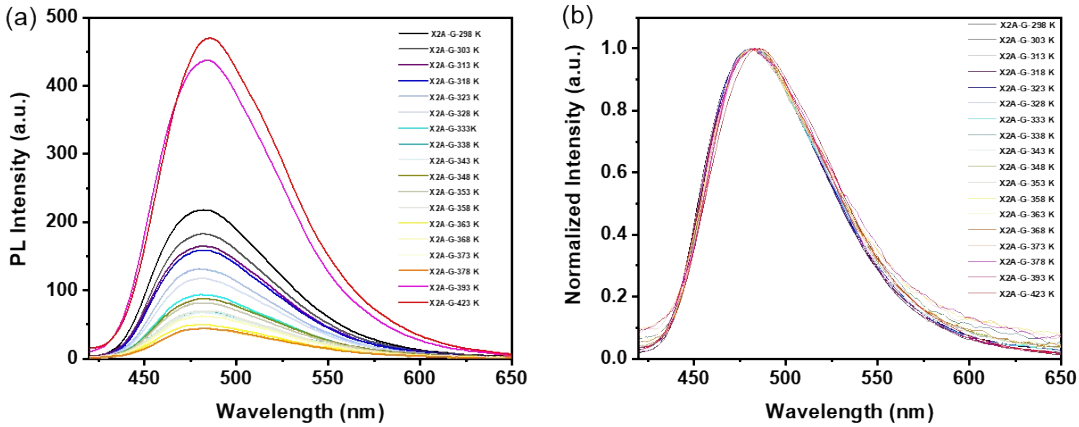

Fig. S41. a) PL spectra and b) Normalized PL spectra of X2A-G crystal with temperature increasing from 298 K to 423 K.

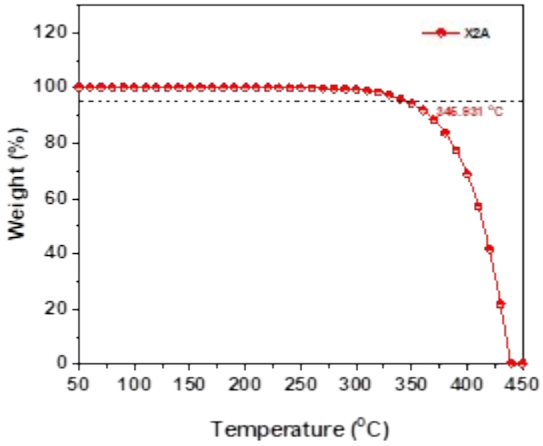

Fig. S42. Thermogravimetric analysis (TGA) analysis of X2A powder.

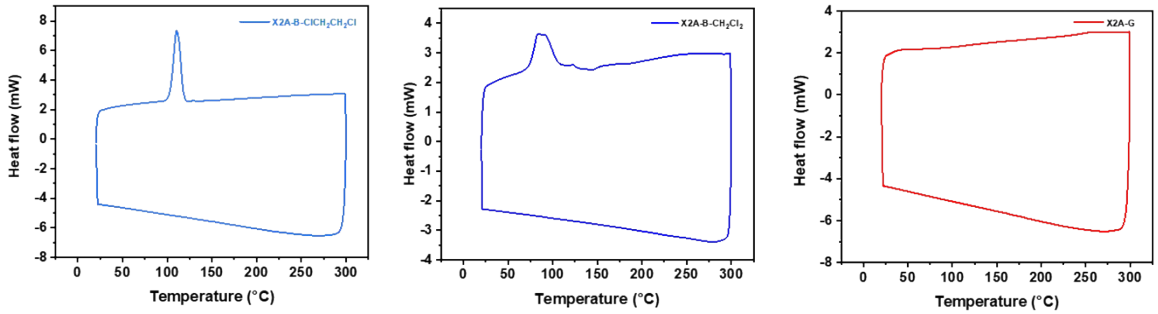

Fig. S43. Differential scanning calorimetry (DSC) curves of X2A-B-$ClCH_2CH_2Cl$, X2A-B-CH_2Cl_2 and X2A-G crystal at the range from 25 °C to 300 °C.

Table S8. Intermolecular interactions between solvent (CH_2Cl_2 and $ClCH_2CH_2Cl$) and anthracene moiety.

Crystal	C-H···π (Å)	Cl-C···π (Å)	C-Cl···π (Å)	Interaction energy (kcal/mol)
X2A-B-CH_2Cl_2	3.001 2.883	3.449	--	5.63
X2A-B-$ClCH_2CH_2Cl$	3.205 2.949	3.605	3.890	4.64

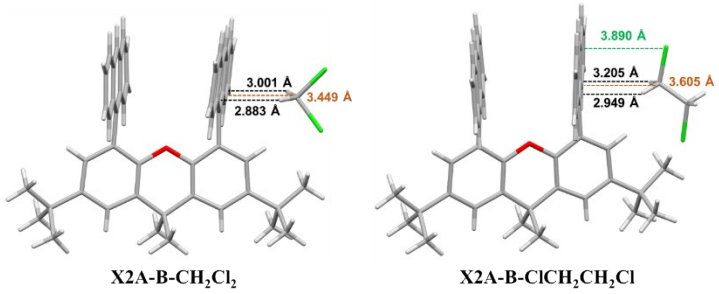

Fig. S44. Distances of intermolecular interactions and calculated interaction energy between solvent (CH_2Cl_2 /$ClCH_2CH_2Cl$) and anthracene moiety in X2A-B-CH_2Cl_2 and X2A-B-$ClCH_2CH_2Cl$ crystals.

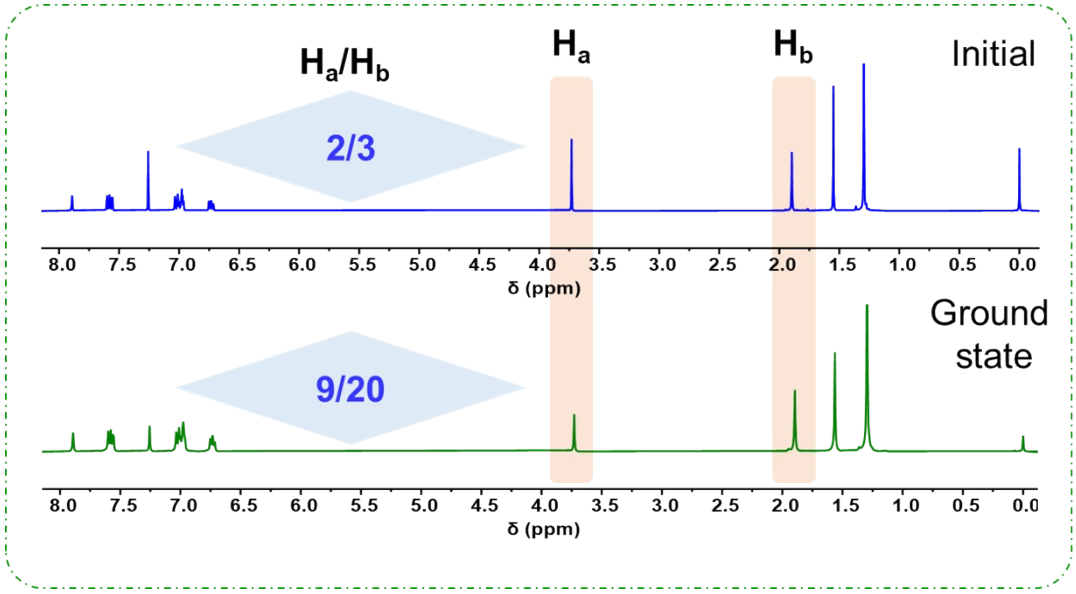

Fig. S45. ^1H NMR spectra of X2A-B-$ClCH_2CH_2Cl$ crystal in $CDCl_3$ at (a) initial and (b) ground state.

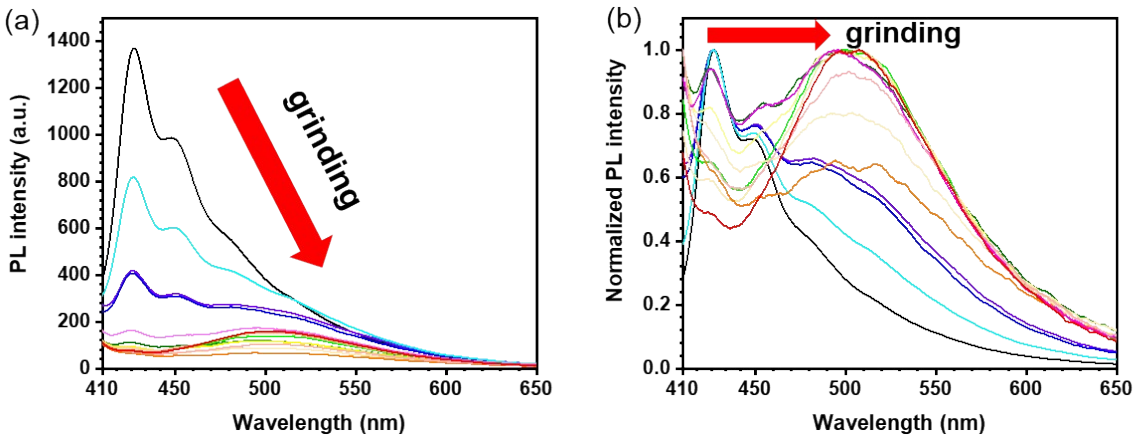

Fig. S46. (a) PL spectra and (b) normalized PL spectra of X2A-B-$ClCH_2CH_2Cl$ crystal upon grinding.

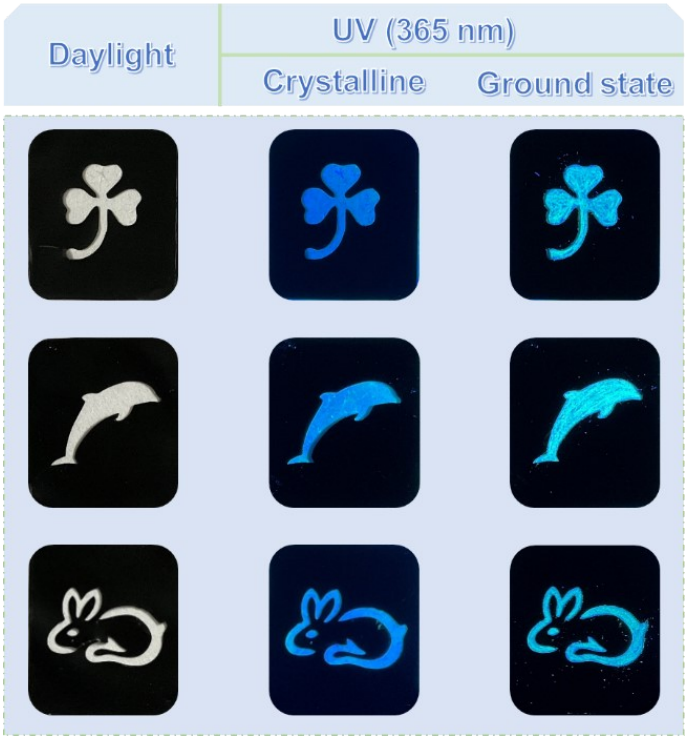

Fig. S47. Patterns constructed by X2A-B microcrystal rapidly obtained from 1, 2-dichloroethane solution. The emission under daylight and 365 nm UV irradiation, the patterns changed from blue emission to green emission after painting.

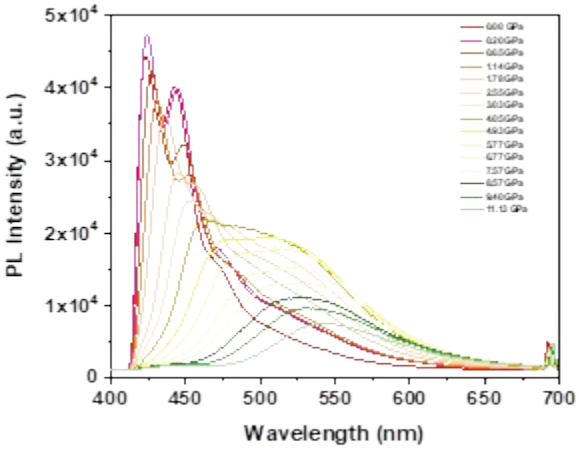

Fig. S48. PL spectra of X2A-B-$ClCH_2CH_2Cl$ crystal with isotropic compression from 0.00 Gpa to 11.13 GPa.

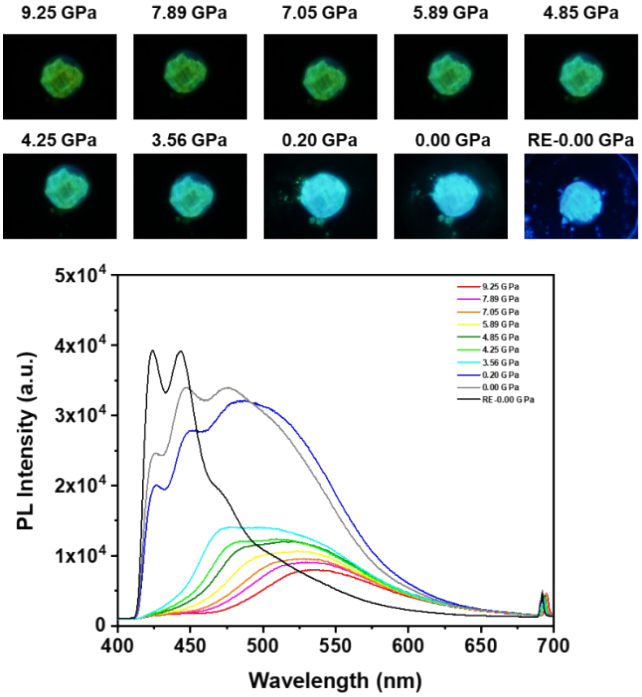

Fig. S49. The fluorescence images and PL spectra of X2A-B-$ClCH_2CH_2Cl$ crystal with the release of pressure from 9.25 GPa.

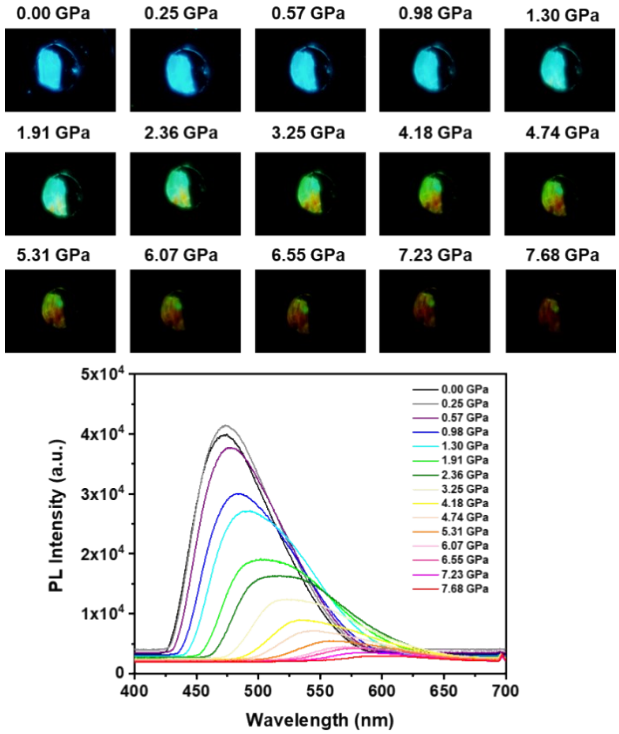

Fig. S50. The fluorescence images and PL spectra of X2A-G crystal with isotropic compression from 0.00 Gpa to 11.13 GPa.

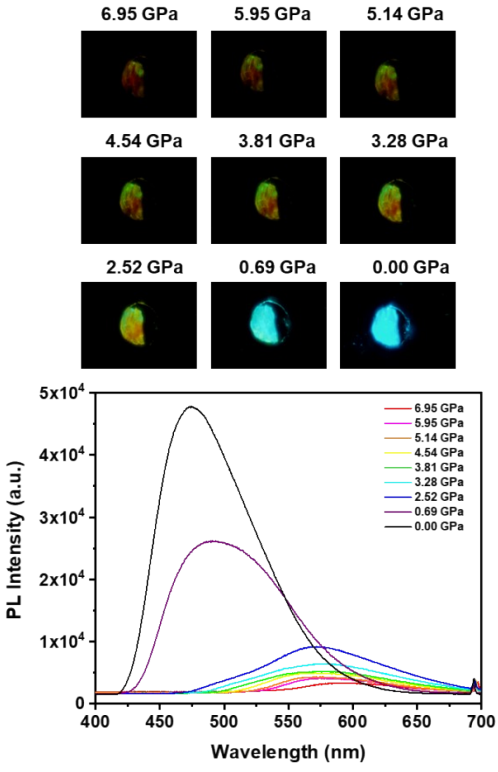

Fig. S51. The fluorescence images and PL spectra of X2A-G crystal with the release of pressure from 6.95 GPa.

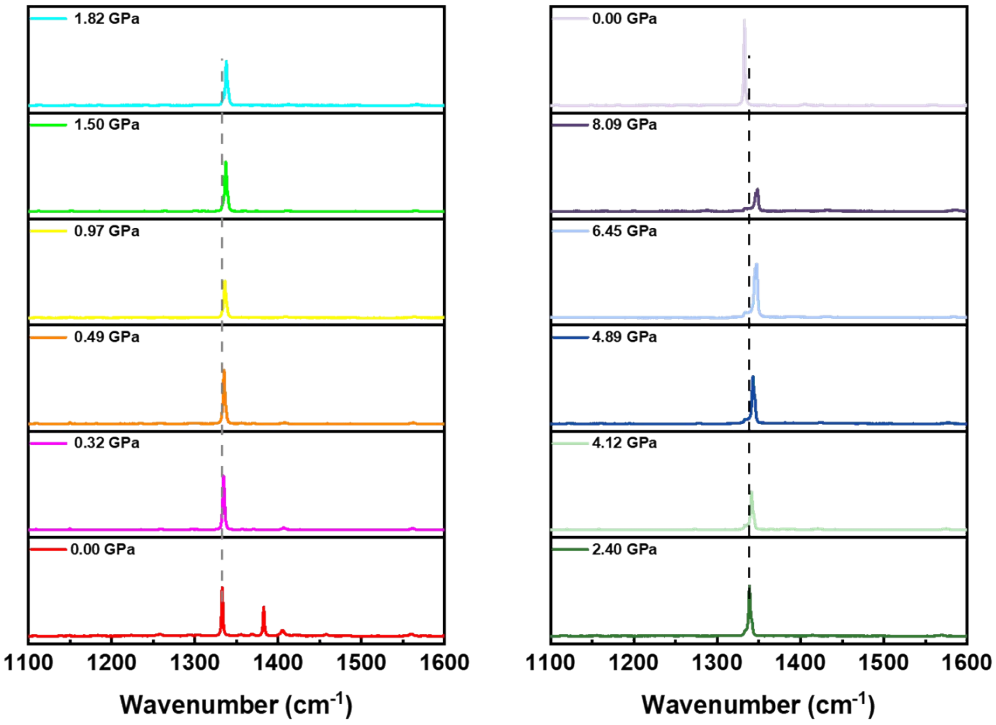

Fig. S52. Raman spectra of X2A-B-$ClCH_2CH_2Cl$ crystal under different pressure with a laser at 785 nm.

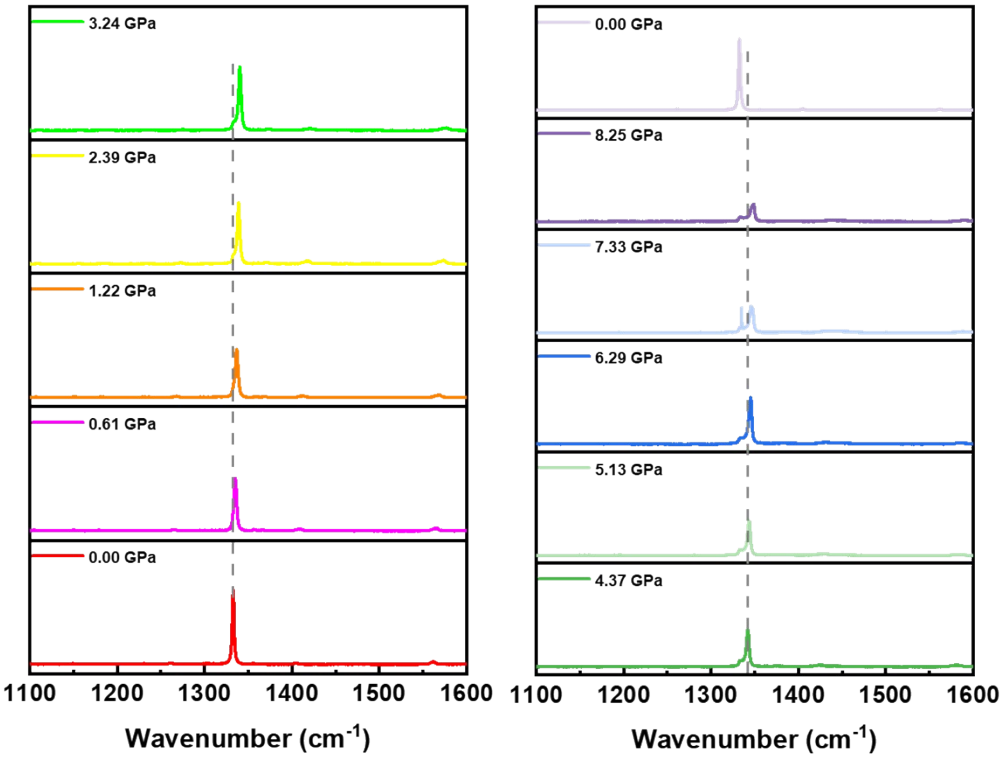

Fig. S53. Raman spectra of X2A-G crystal under different pressure with a laser at 785 nm.

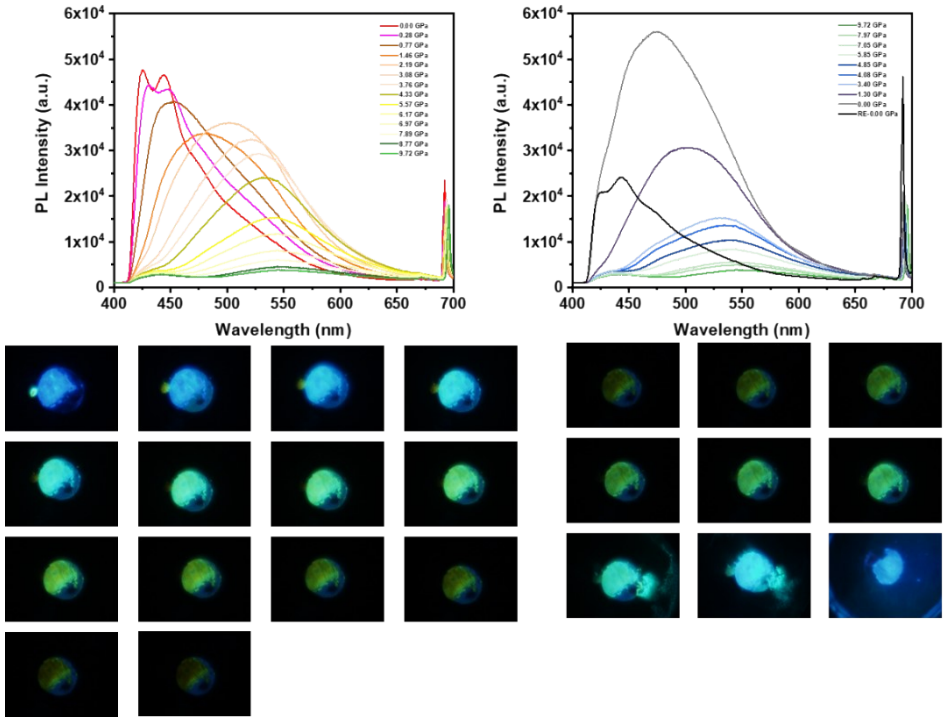

Fig. S54. The fluorescence images and PL spectra of X2A-B-CH_2Cl_2 crystal with (a) isotropic compression from 0 Gpa to 9.72 Gpa and (b) the release of pressure from 9.72 GPa.

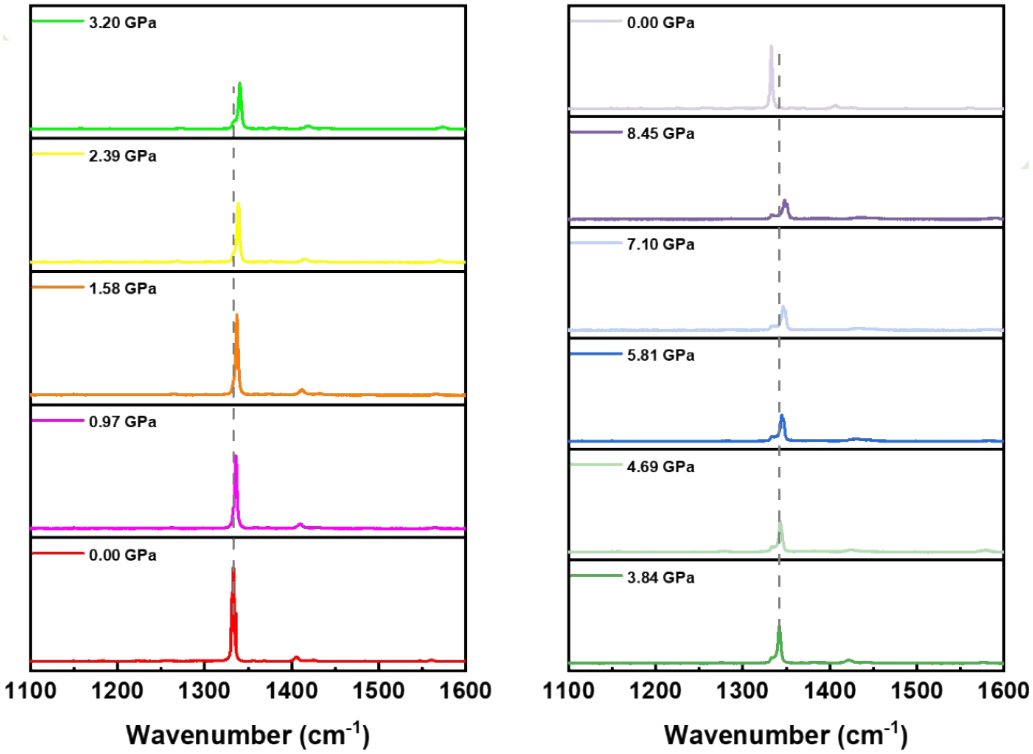

Fig. S55. Raman spectra of X2A-B-CH_2Cl_2 crystal under different pressure with a laser at 785 nm.

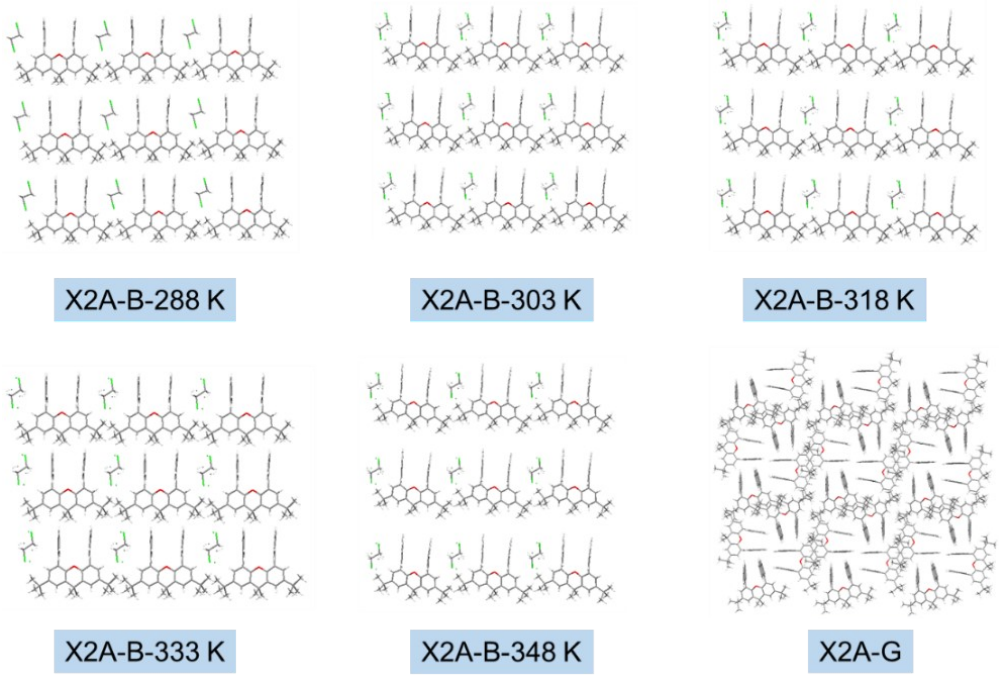

Fig. S56. Molecular packing modes of X2A-B-$ClCH_2CH_2Cl$ crystals at different temperature (288 K, 303 K, 318 K, 333 K, 348 K) and X2A-G crystal.

Table S9. Summary data of molecular configuration with angles and distance between anthryl planes of X2A-B-$ClCH_2CH_2Cl$ crystals at different temperature (288 K, 303 K, 318 K, 333 K, 348 K) and X2A-G crystal.

crystal	θ_1(˚)	θ_2(˚)		θ_2 average (˚)	θ_3(˚)	d_P(Å)		d_P average (Å)	d_c(Å)	CCDC Number
X2A-B-288 K	0.90	70.58	70.49	70.54	4.89	4.340	4.340	4.340	4.618	2180361
X2A-B-303 K	0.96	70.76	70.67	70.72	4.72	4.335	4.333	4.334	4.608	2180362
X2A-B-318 K	0.96	70.98	70.94	70.96	4.50	4.332	4.328	4.330	4.598	2180372
X2A-B-333 K	0.99	71.22	71.19	71.21	4.32	4.329	4.322	4.326	4.589	2180373
X2A-B-348 K	1.05	71.48	71.57	71.53	4.09	4.324	4.319	4.322	4.581	2180374
X2A-G	3.99	68.86	73.99	71.43	12.83	3.760	3.635	3.698	3.935	2180353

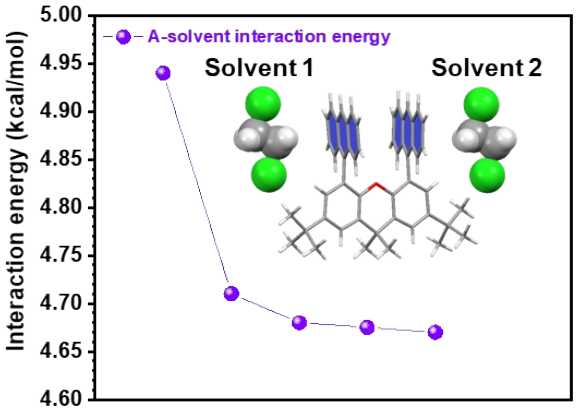

Fig. S57. Interaction energy between anthracene moieties and 1, 2-dichloroethane molecules of X2A-B-$ClCH_2CH_2Cl$ crystals at different temperature (288 K, 303 K, 318 K, 333 K, 348 K).

Table S10. Summary data of interaction energy between anthracene moieties and anthracene moiety with 1, 2-dichloroethane molecules of X2A-B-$ClCH_2CH_2Cl$ crystals at different temperature (288 K, 303 K, 318 K, 333 K, 348 K) and X2A-G crystal.

Crystal	A-A energy (kcal/mol)	A-Solvent 1 (kcal/mol)	A-Solvent 2 (kcal/mol)	A-Solvent average (kcal/mol)
X2A-B-288 K	4.83	4.87	5.01	4.94
X2A-B-303 K	4.88	4.61	4.81	4.71
X2A-B-318 K	4.91	4.57	4.79	4.68
X2A-B-333 K	4.94	4.58	4.77	4.68
X2A-B-348 K	4.99	4.59	4.75	4.67
X2A-G	8.47	--	--	--

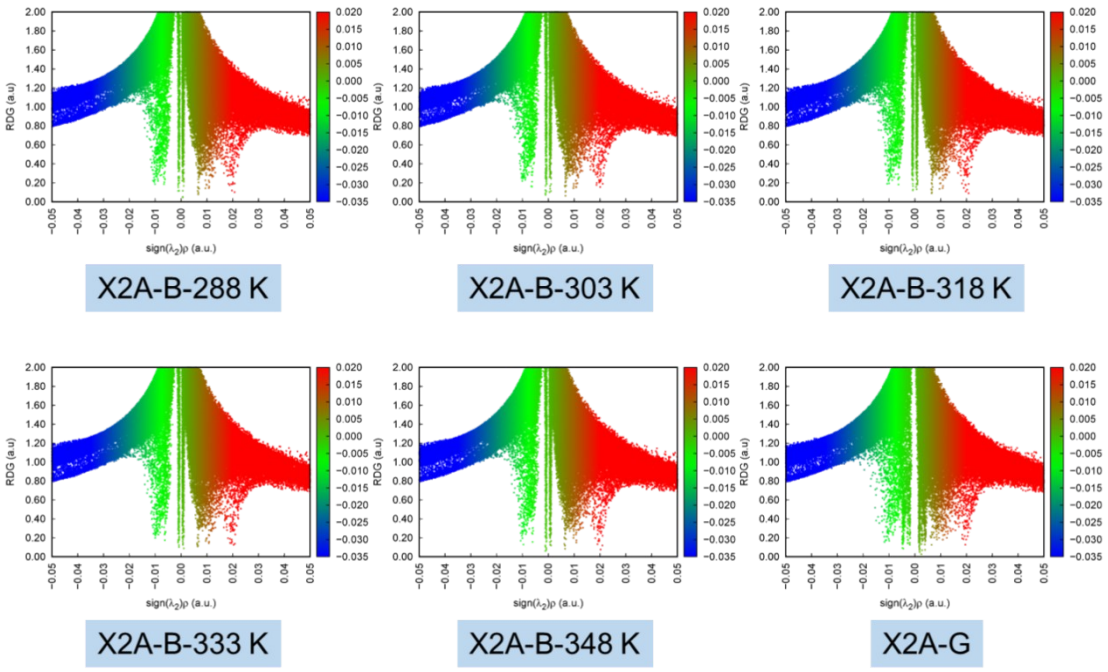

Fig. S58. The scatter diagram for RDG versus sign (λ2) ρ of X2A-B-$ClCH_2CH_2Cl$ crystals at different temperature (288 K, 303 K, 318 K, 333 K, 348 K) and X2A-G crystal.

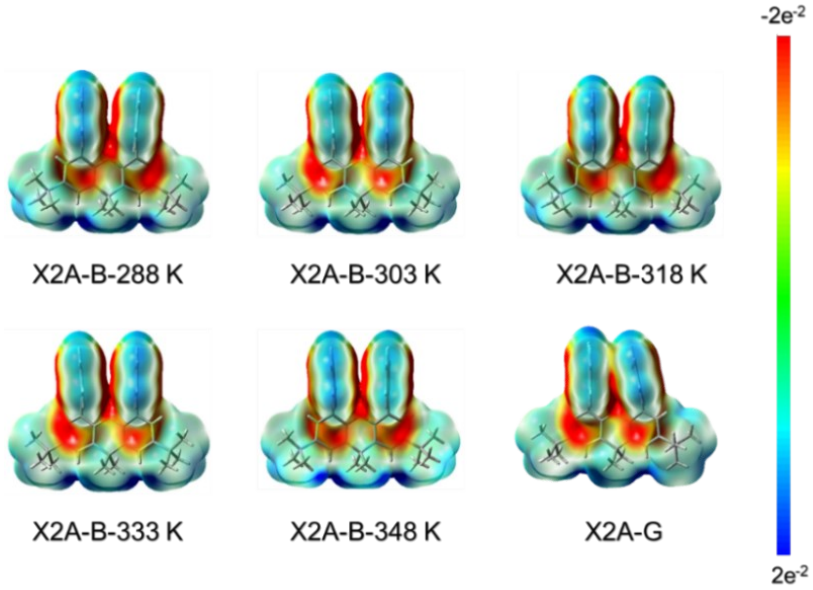

Fig. S59. Electrostatic potential (ESP) analysis of X2A-B-$ClCH_2CH_2Cl$ crystals at different temperature and X2A-G crystal (the geometry were extracted from single crystal).

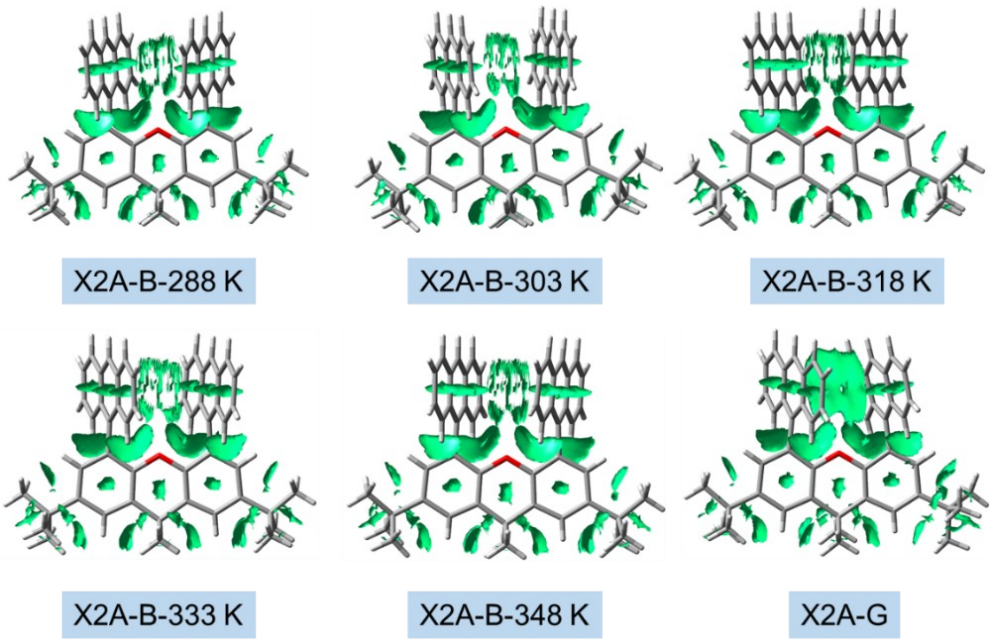

Fig. S60. Gradient isosurfaces for X2A-B-$ClCH_2CH_2Cl$ crystals at different temperature (288 K, 303 K, 318 K, 333 K, 348 K) and X2A-G crystal.

Table S11. Transfer integrals of X2A-B-$ClCH_2CH_2Cl$ crystals at different temperature (288 K, 303 K, 318 K, 333 K, 348 K) and X2A-G crystal.

Crystal	A_H--B_H (meV)
X2A-B-288 K	17.38
X2A-B-303 K	18.41
X2A-B-318 K	19.88
X2A-B-333 K	21.48
X2A-B-348 K	23.30
X2A-G	108.53

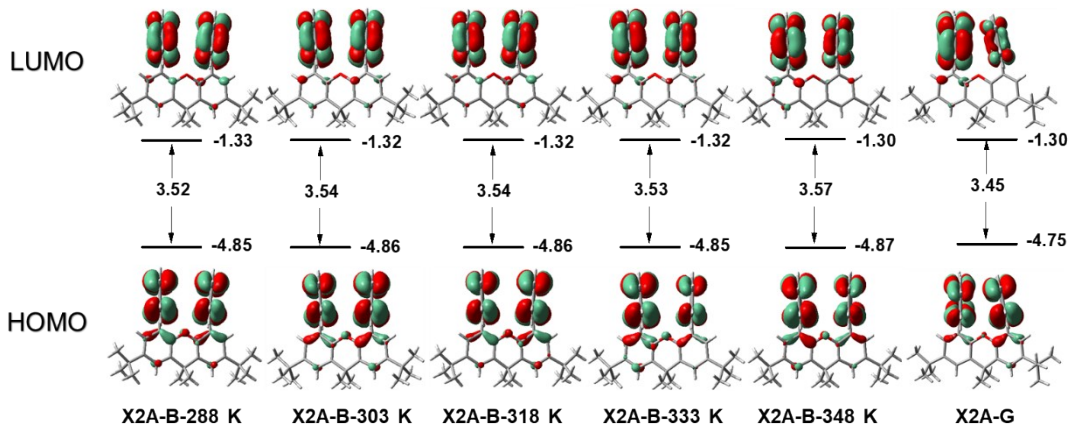

Fig. S61. HOMO, LUMO orbits of X2A-B-$ClCH_2CH_2Cl$ crystals at different temperature and X2A-G crystal (the geometry were extracted from single crystal).

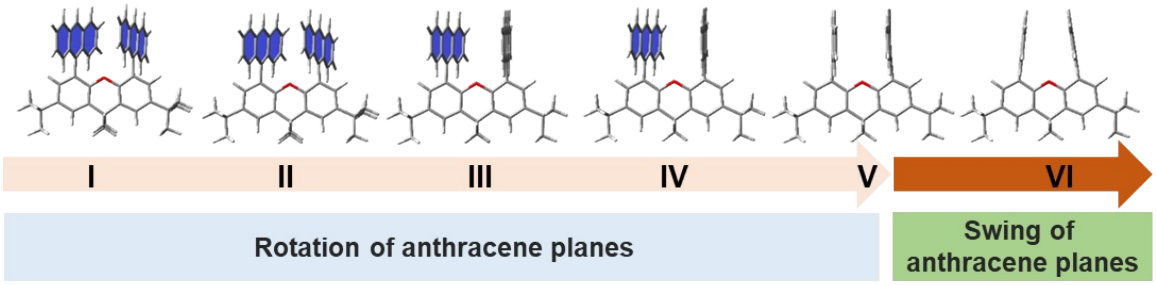

Fig. S62. The geometries of I-VI at excited state, which can be divided to two steps (rotation of anthracene planes and swing of anthracene planes).

References

1. Gaussian 16, Revision C.01, M. J. Frisch, G. W. Trucks, H. B. Schlegel, G. E. Scuseria, M. A. Robb, J. R. Cheeseman, G. Scalmani, V. Barone, G. A. Petersson, H. Nakatsuji, X. Li, M. Caricato, A. V. Marenich, J. Bloino, B. G. Janesko, R. Gomperts, B. Mennucci, H. P. Hratchian, J. V. Ortiz, A. F. Izmaylov, J. L. Sonnenberg, D. Williams-Young, F. Ding, F. Lipparini, F. Egidi, J. Goings, B. Peng, A. Petrone, T. Henderson, D. Ranasinghe, V. G. Zakrzewski, J. Gao, N. Rega, G. Zheng, W. Liang, M. Hada, M. Ehara, K. Toyota, R. Fukuda, J. Hasegawa, M. Ishida, T. Nakajima, Y. Honda, O. Kitao, H. Nakai, T. Vreven, K. Throssell, J. A. Montgomery, Jr., J. E. Peralta, F. Ogliaro, M. J. Bearpark, J. J. Heyd, E. N. Brothers, K. N. Kudin, V. N. Staroverov, T. A. Keith, R. Kobayashi, J. Normand, K. Raghavachari, A. P. Rendell, J. C. Burant, S. S. Iyengar, J. Tomasi, M. Cossi, J. M. Millam, M. Klene, C. Adamo, R. Cammi, J. W. Ochterski, R. L. Martin, K. Morokuma, O. Farkas, J. B. Foresman, and D. J. Fox, Gaussian, Inc., Wallingford CT, 2019.
2. Tian Lu, Feiwu Chen, Multiwfn: A Multifunctional Wavefunction Analyzer, *J. Comput. Chem.* **33**, 580-592 (2012).